NAVAL POSTGRADUATE SCHOOL
Monterey, California

THESIS

EFFECTS OF THERMOBARICITY ON COUPLED ICE-MIXED LAYER THERMODYNAMICS

by

Mathias K. Roth

June 2003

Thesis Advisor:	Roland W. Garwood
Second Reader:	Arlene Guest

Approved for public release; distribution is unlimited.

THIS PAGE INTENTIONALLY LEFT BLANK

REPORT DOCUMENTATION PAGE			Form Approved OMB No. 0704-0188
Public reporting burden for this collection of information is estimated to average 1 hour per response, including the time for reviewing instruction, searching existing data sources, gathering and maintaining the data needed, and completing and reviewing the collection of information. Send comments regarding this burden estimate or any other aspect of this collection of information, including suggestions for reducing this burden, to Washington headquarters Services, Directorate for Information Operations and Reports, 1215 Jefferson Davis Highway, Suite 1204, Arlington, VA 22202-4302, and to the Office of Management and Budget, Paperwork Reduction Project (0704-0188) Washington DC 20503.			
1. AGENCY USE ONLY *(Leave blank)*	**2. REPORT DATE** June 2003	**3. REPORT TYPE AND DATES COVERED** Master's Thesis	
4. TITLE AND SUBTITLE: Title (Mix case letters) Effects of thermobaricity on coupled ice-mixed layer thermodynamics.			**5. FUNDING NUMBERS**
6. AUTHOR(S) Mathias K. Roth			
7. PERFORMING ORGANIZATION NAME(S) AND ADDRESS(ES) Naval Postgraduate School Monterey, CA 93943-5000			**8. PERFORMING ORGANIZATION REPORT NUMBER**
9. SPONSORING /MONITORING AGENCY NAME(S) AND ADDRESS(ES) N/A			**10. SPONSORING/MONITORING AGENCY REPORT NUMBER**
11. SUPPLEMENTARY NOTES The views expressed in this thesis are those of the author and do not reflect the official policy or position of the Department of Defense or the U.S. Government.			
12a. DISTRIBUTION / AVAILABILITY STATEMENT Approved for public release; distribution is unlimited.			**12b. DISTRIBUTION CODE** A

13. ABSTRACT ***(maximum 200 words)***

The unique properties of the temperature and salinity profiles for polar oceans are critical for high-latitude mixed layer thermodynamics. In the Polar regions the water column is coldest and freshest at the surface where ice may be present. This density structure often leads to entrainment and affects both the mixed layer depth and the ice thickness.

Thermobaricity, the combined dependence of seawater thermal expansion on temperature and pressure, magnifies the buoyancy flux associated with mixed layer convection. When thermobaricity amplifies entrainment so that the heat into the mixed layer is greater than the heat leaving the water column, the mixed layer warms and any existing ice begins to melt. Similarly, if the heat entrained is less than the heat leaving the column, the mixed layer cools and freezing occurs at the surface. In the former situation a polynya, or region of no ice surrounded by ice coverage, may form.

A one-dimensional vertical model is built, and trial cases are run to show the intricate relationships that govern the heat and salt fluxes and subsequent ice thickness. The model shows the importance of thermobaricity to the air-sea-ice interactions. It also offers significant insight into how relatively constant atmospheric forcing can lead to polynya-like conditions.

14. SUBJECT TERMS Mixed Layer, Thermobaricity, Entrainment, Polynya			**15. NUMBER OF PAGES 77**
			16. PRICE CODE
17. SECURITY CLASSIFICATION OF REPORT Unclassified	**18. SECURITY CLASSIFICATION OF THIS PAGE** Unclassified	**19. SECURITY CLASSIFICATION OF ABSTRACT** Unclassified	**20. LIMITATION OF ABSTRACT** UL

NSN 7540-01-280-5500 Standard Form 298 (Rev. 2-89)
Prescribed by ANSI Std. 239-18

THIS PAGE INTENTIONALLY LEFT BLANK

Approved for public release; distribution is unlimited

EFFECTS OF THERMOBARICITY ON COUPLED ICE-MIXED LAYER THERMODYNAMICS

Mathias K. Roth
Ensign, United States Navy
B.S., United States Naval Academy, 2002

Submitted in partial fulfillment of the
requirements for the degree of

MASTER OF SCIENCE IN PHYSICAL OCEANOGRAPHY

from the

NAVAL POSTGRADUATE SCHOOL
June 2003

Author: Mathias K. Roth

Approved by: Roland W. Garwood
Thesis Advisor

Arlene Guest
Second Reader

Mary Batteen
Chairman, Department of Oceanography

THIS PAGE INTENTIONALLY LEFT BLANK

ABSTRACT

The unique properties of the temperature and salinity profiles for polar oceans are critical for high-latitude mixed layer thermodynamics. In the Polar regions the water column is coldest and freshest at the surface where ice may be present. This density structure often leads to entrainment and affects both the mixed layer depth and the ice thickness.

Thermobaricity, the combined dependence of seawater thermal expansion on temperature and pressure, magnifies the buoyancy flux associated with mixed layer convection. When thermobaricity amplifies entrainment so that the heat into the mixed layer is greater than the heat leaving the water column, the mixed layer warms and any existing ice begins to melt. Similarly, if the heat entrained is less than the heat leaving the column, the mixed layer cools and freezing occurs at the surface. In the former situation a polynya, or region of no ice surrounded by ice coverage, may form.

A one-dimensional vertical model is built, and trial cases are run to show the intricate relationships that govern the heat and salt fluxes and subsequent ice thickness. The model shows the importance of thermobaricity to the air-sea-ice interactions. It also offers significant insight into how relatively constant atmospheric forcing can lead to polynya-like conditions.

THIS PAGE INTENTIONALLY LEFT BLANK

TABLE OF CONTENTS

THIS PAGE INTENTIONALLY LEFT BLANK

LIST OF FIGURES

THIS PAGE INTENTIONALLY LEFT BLANK

ACKNOWLEDGMENTS

I would very much like to thank Dr. Roland W. Garwood for all of the time and effort he put forth to make this project a successful one. His tutoring and guidance have made this thesis possible, and his mentorship has been invaluable. I am grateful to Arlene Guest, who was an irreplaceable source of both insight and advice. Thank you to Dr. Peter Guest, who graciously agreed to assist me with information and resources in relation to high-latitude meteorology, and Dr. Robert Bourke, who likewise assisted me with high-latitude oceanographic research. This research is supported in part by the office of Naval Research Code 322HL, and this support is gratefully acknowledged. I would also like to thank my wife, Amy, for all of her support throughout this process.

I. INTRODUCTION

Freezing and melting of ice in the Arctic and Antarctic environments are determined by the thermodynamic fluxes among air, sea-ice, and oceanic mixed layer. The energy exchanged among these three domains is in a delicate balance that may theoretically lead to an ice-free Arctic basin or another ice age in the limits. This paper will focus primarily on high-latitude ice-mixed layer dynamics in both the northern and southern hemispheres. Although the vertical energy fluxes within these regions are governed by similar underlying physics one dimensionally, the two polar regions have differences. One phenomenon possible in all polar regions is the polynya.

Polynyas may form as a local extreme state on a small scale, without major large-scale or basin changes. As local extremes, polynyas are a potential laboratory for climate change. Thus, part of the of the impetus for this research is stated clearly by Smith *et al.* (1990), "At predictable, recurrent locations throughout the polar regions, there are oceanic areas which remain either partially or totally ice free at times and under climatological conditions where we would expect the water to be ice covered." Conversely, ice may also form in these regions at times when climatological conditions might warrant no-ice conditions. Simply put, there is more to ice formation and melting than climatological conditions; the understanding of the dynamics and thermodynamics of the water column below and coupled with the ice needs to be explicitly included into prediction models.

This work has many implications for the United States Navy both for now and in the future. For the present time a better understanding of the physics of the mixed layer will improve ice thickness and ice extent forecast models like PIPS (Preller *et al.,* 2002). The output from such a model could be vital for submarine and or shipping operations in high-latitude regions. Furthermore, information gained from these models could improve mission effectiveness and efficiency while preventing the wasting of valuable resources like equipment, time, and money. For example, if a scenario were developed where a P3-Orion was required to lay sonobuoys in the Barents Sea it would be very useful in the planning stages of this mission to have information regarding the ice coverage. If the

region is ice covered, an ice penetrating sonobuoy would be very useful assuming the thickness of the ice does not exceed the burying capabilities of the sonobuoy. However, if the region were either ice-free or the ice were too thick then the employment of this type of sonobuoy would be a waste of time and equipment. Similarly, the use of a conventional sonobuoy in an ice-covered region would be useless. Either way real-time knowledge about the ice thickness and extent would be invaluable for the planning of this mission.

The long-term importance of this study, for the Navy, may go beyond forecast capabilities and mission effectiveness to include macro-scale circulation and deep water formation. The same physical processes that are explored in this work as mechanisms for ice formation and melting also seemingly play a significant role in taking oxygen and nutrients from the surface and reintroducing them back into the water column. When these nutrients are returned deep in the water column they flow with the denser water as it spreads around the globe replenishing the world's oceans. Understanding completely how this process works and the resulting ramifications for oceanic and atmospheric forecasts could provide a decisive tactical advantage.

Chapter II explores the regional descriptive oceanography of the high latitudes. Climatology, basin circulation patterns, and polynya events are discussed in this chapter. Following this background discussion, Chapter III delves into the physics of the coupled ice-mixed layer system, examining both previous scientific studies and the current work. Requirements for the accurate modeling of this physics are also discussed. Chapter IV reviews sensitivity studies, as the strengths and weaknesses of this model are discovered. Finally, Chapter V provides a summary of this work and details the conclusions drawn as well as recommendation for work that needs to be continued.

II. POLAR REGIONS

This section is designed to provide the background knowledge that is important for the air-sea-ice model. The focus of the circulation section is on the Arctic since the flow patterns in the Northern Hemisphere are much more complex than the circulation patterns in the Southern Hemisphere. It is, however, important to note that the Weddell Polynya in Antarctica appeared to migrate west from year to year during its presence in the 1970s. Despite this fact, for the purposes of the one-dimensional vertical model, it is assumed that if the model can handle the horizontal advective effects of the Arctic, it is robust enough to handle similar effects in the Antarctic. In regards to climate, similar assumptions cannot be made since the atmospheric forcing can be significantly more extreme in the Antarctic than in the Arctic. The section concerning leads and polynyas focuses primarily on the Weddell Polynya in the Antarctic. The reason for this is not because physics does not support polynyas in the Arctic, but simply because the relatively large amount of information about the Weddell Polynya makes it a good example of and laboratory for the physics that create ice-free regimes in an ice-covered region.

A. CIRCULATION OF THE ARCTIC OCEAN

To better understand one-dimensional vertical effects in the Arctic Ocean, the horizontal movement of water into and through the region, as well as the bathymetry of the region need to be discussed (Fig. 1). For the purposes of this paper the rather complex circulation patterns and bottom topography of the Arctic Ocean examined by Rudels *et al.* (1994) is simplified to include two primary basins, the Eurasian Basin and the Canadian Basin, the Lomonosov Ridge, and the flow of water between and around these features. This simplification is justified since Rudels *et al.* (1994) demonstrate a strong front between the two basins at the Lomonosov Ridge. Similarly, Aagaard and Carmack (1994) show evidence to support the presence of a strong boundary current around the Lomonosov Ridge.

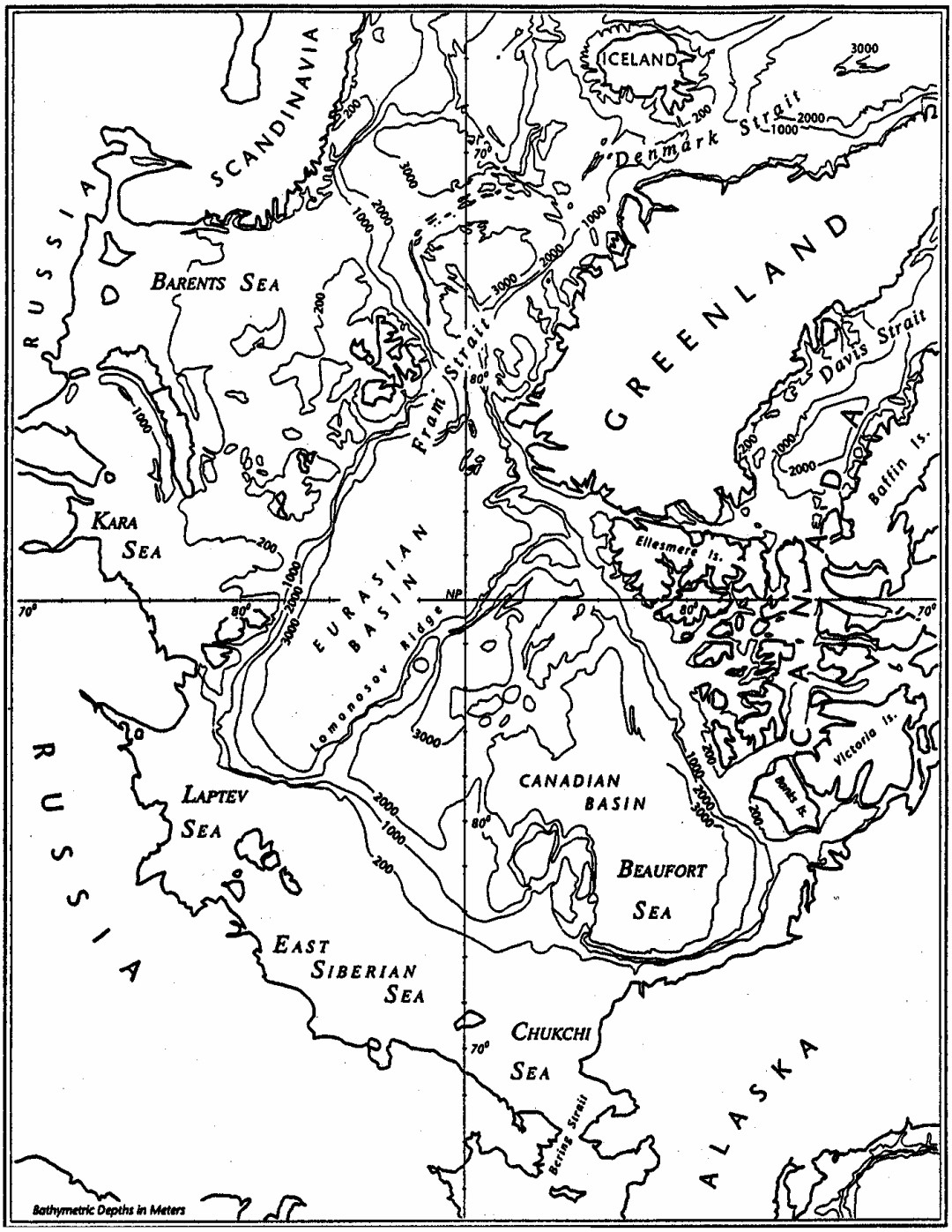

Figure 1. The Arctic Ocean with bathymetry. From Barry *et al.*, 1993.

Although water can enter and leave the Arctic Ocean from several points, the Bering Strait will be considered the primary point of entry for Pacific water per Aagaard and Carmack (1994). Likewise, the Fram Strait was considered the main source for Atlantic and Intermediate waters according to Rudels *et al*. (1994). A secondary source of water into the Arctic is river runoff that can act to cap a water column and prevent heat exchange with the environment (Mellor and Hakkinen, 1994).

Despite their proximity to one another, the two basins are different. Rudels *et al.* (1994) suggest that the circulation through the Canadian Basin is slower than that of the Eurasian Basin, causing the water to reside in the Canadian Basin by as much as a decade longer than in the Eurasian Basin. Rudels *et al.* (1994) show the Canadian Basin to be well mixed according to temperature and salinity by water type. Rudels *et al.* (1994) also depict the Eurasian Basin as being well mixed according to temperature and salinity by water type. However, the Atlantic and intermediate waters of the Eurasian Basin increase in both temperature and salinity as depth increases, whereas the same type of water in the Canadian Basin decreases in both temperature and salinity as depth increases (Rudels *et al.*, 1994). This difference is important to the vertical heat flux and convection of each basin respectively. Similarly, the difference is important when water from both basins come together at the Lomonosov Ridge because double diffusion may occur (Rudels *et al.*, 1994).

The circulation time is shorter in the Eurasian Basin than the Canadian Basin because advection is strong enough in the Eurasian Basin to pass the incoming water back out of the Fram Strait (Rudels *et al.,* 1994). That does not mean that vertical processes do not occur in this basin. In fact, the temperature and salinity profiles detailed by Rudels *et al.* (1994) could allow entrainment of warmer underlying water into the colder surface layer. If this were to occur, the rising heat could melt ice. At the same time, the loss of heat at depth would cool the lower layers.

The temperature and salinity structure of the Canadian Basin is of particular interest since Rudels *et al.* (1994) suggest that the structure will allow heat to be mixed down into the water column (Fig. 2). Mixing of heat down into the water column would deepen the mixed layer.

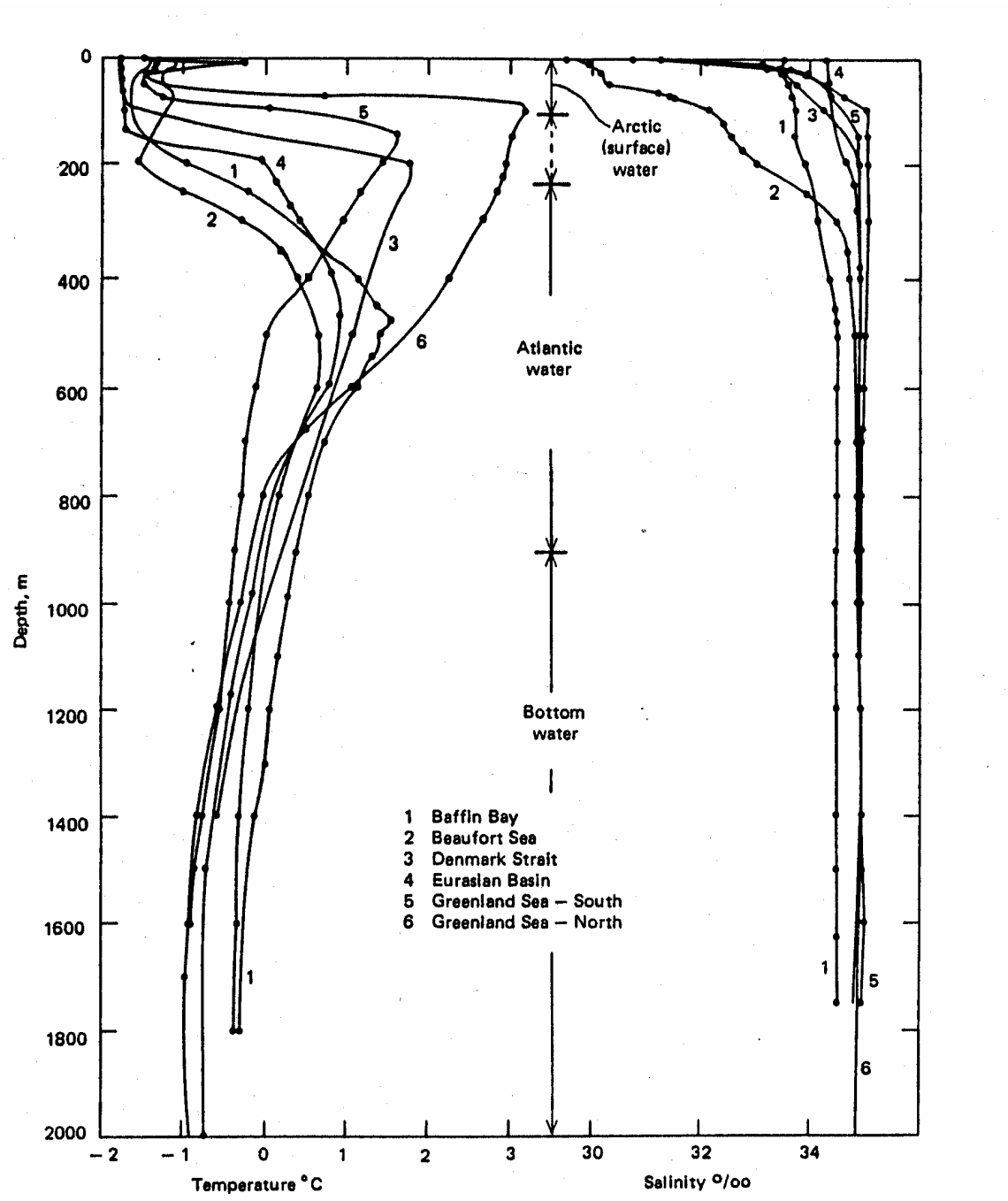

Figure 2. Representative temperature and salinity profiles from various locations in the Northern Hemisphere high latitudes. From Coachman and Aagaard, 1974.

If this mixing of heat down is greater than the entrainment up from the abyss,* or if the basin is not deep enough for an abyss to exist, then little heat would be added to the mixed layer to melt ice. If, however, ice forms because entrained heat is less than heat lost to the atmosphere, the mixed layer salinity increases. Increased salinity would then make the water sink convectively. This process creates the warm and salty water at depth discussed by Aagaard and Carmack (1994).

Introducing advective processes like river runoff or narrow currents like the West Spitsbergen Current, as mentioned by Mellor and Hakkinen (1994), probably do little to offset the vertical processes in the Canadian Basin. River runoff would create fresh water at the surface that would quickly freeze and add to the ice. Currents at either the surface or some depth could create eddies and cause stirring in the horizontal. However, due to the stronger mixing of heat down in the column, these eddies would have little effect on the direction of vertical mixing.

Advective processes like friction, wind stress, and currents undoubtedly keep the ice in the Canadian Basin from growing unbounded. Similarly, Lemke *et al.* (1990) point out that a deep mixed layer can resist ice growth. This situation would be very similar to the circumstances surrounding the presence of a polynya. However, strong mixing of heat down in the Canadian Basin could theoretically make it a one-dimensional ice generator, especially when the temperature of the water at the surface is at or near the freezing point. As it is, the Canadian Basin becomes a density capacitor, building up density over longer periods of time and then slowly but constantly discharging salty and relatively warm water at the Lomonosov Ridge. This water then mixes with cooler and fresher water released from the Eurasian Basin. When the waters from the two basins come in contact at the Lomonosov Ridge double diffusion may occur as noted above. Strong boundary currents along the Lomonosov Ridge and the east coast of Greenland then push and carry the water before it exits from the Fram Strait at depth (Aagaard and Carmack, 1994). Stable water, defined as cold salty water beneath warm fresher water, is the ultimate result of the double diffusion. In this way warm, salty, cold, and fresh waters

* The term abyss is borrowed from Hakkinen (1987) and is used here to mean the depth of the water column beneath the mixed layer.

are all brought into the Arctic Ocean, split and processed by both the topography and circulation, and then re-circulated to replenish the world's oceans (Fig. 3).

B. ATMOSPHERIC CONDITIONS

Atmospheric forcing plays a role in both the northern and southern hemispheres. Ultimately, ice will form or melt as a result of the overall energy balance. This balance includes radiation fluxes, sensible heat, and latent heat (Fig. 4) in both polar regions. Whether open areas like leads exist, when heat is brought to the surface, is critical to the energy balance since Vihma (1995) states that ice cover prevents heat exchange. Okada and Yamanouchi (1995) similarly show that when the sea ice concentration increases in the Antarctic winter the surface heat flux decreases. If a large section of ice in the South Pole were instantaneously removed, evidence presented by Wu *et al.,* (1996) suggests that the energy balance would restore the ice within one year. This not only demonstrates the strength of the energy balance but also suggests a seasonality to ice formation.

Seasonal change is also an important factor in the overall energy balance. Sea ice concentration is greatest in the southern hemisphere in the July to August time frame during the Antarctic winter (Fig. 5). Similarly, the sea ice extent is greatest in the northern hemisphere from February to March during the Arctic winter (Fig. 6). Seasonal differences can be witnessed, and melting and freezing can be observed through surface albedo. A low albedo, measured in percentage, corresponds to melting ice and a high albedo classifies solid ice (Barry *et al.,* 1993).

There are also significant seasonal differences in ice coverage within each of the polar regions. Preller *et al.* (2002) describe ice coverage in Arctic regions to be thinnest during the summer; from June to September, and thickest in the winter; from March to April. Similarly, Preller *et al.* (2002) suggest that different seas, within the Arctic, for a given season will have different ice thickness and coverage, but that no sea will perpetually have the greatest coverage. Preller *et al.* (2002) compare this phenomenon to a seesaw where for a given summer sea "A" has thicker ice than sea "B", but the following summer sea "B" will have greater thickness than sea "A".

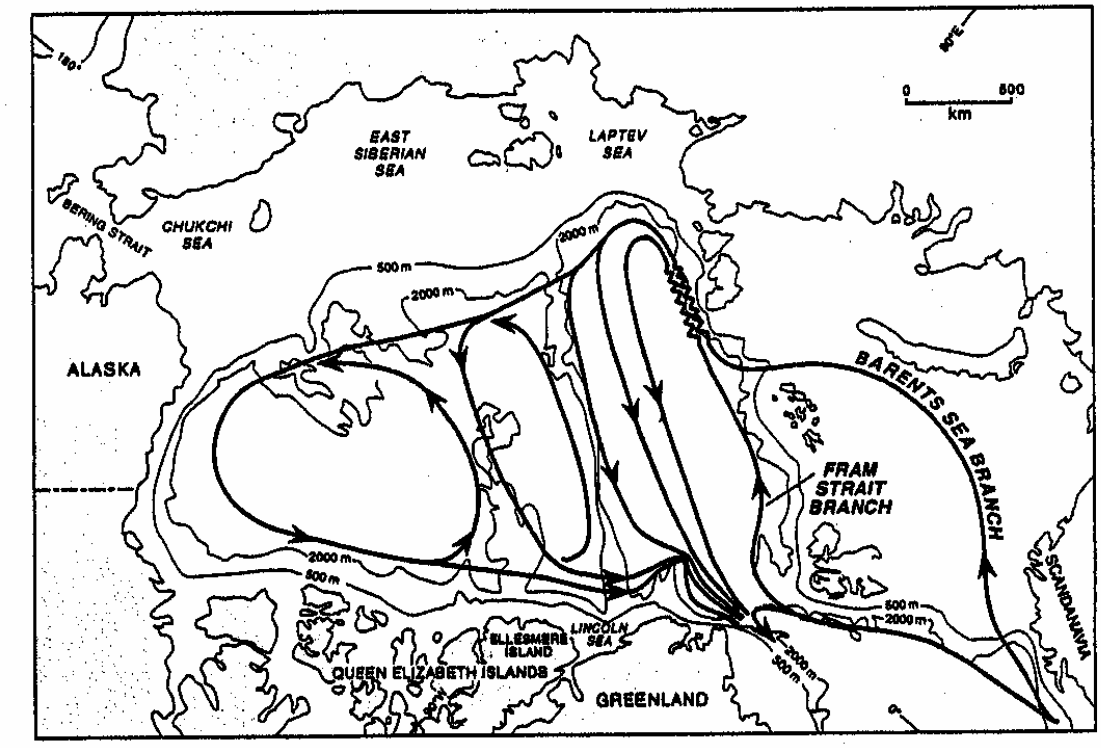

Figure 3. Circulation of the Atlantic Layer and intermediate depth waters of the Arctic Ocean. From Rudels *et al.*, 1994.

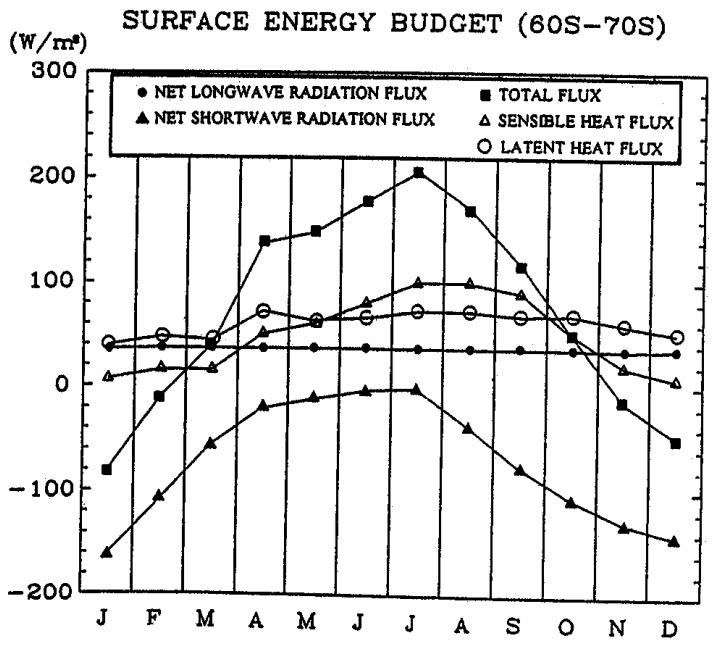

Figure 4. Typical annual surface energy budget for the Southern Hemisphere. From Okada and Yamanouchi, 1995.

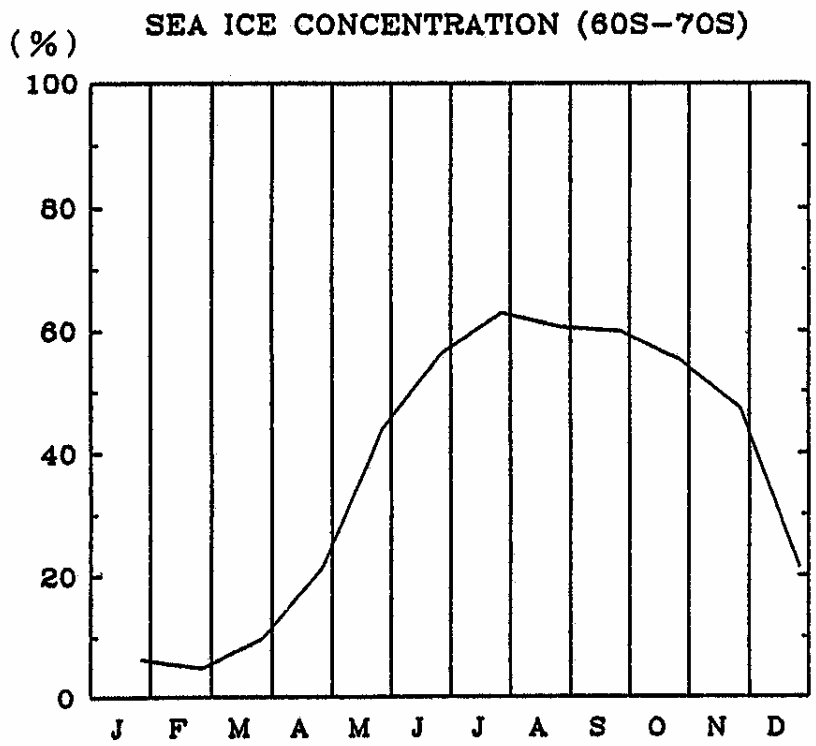

Figure 5. Typical annual Southern Hemisphere sea ice concentration. From Okada and Yamanouchi, 1995.

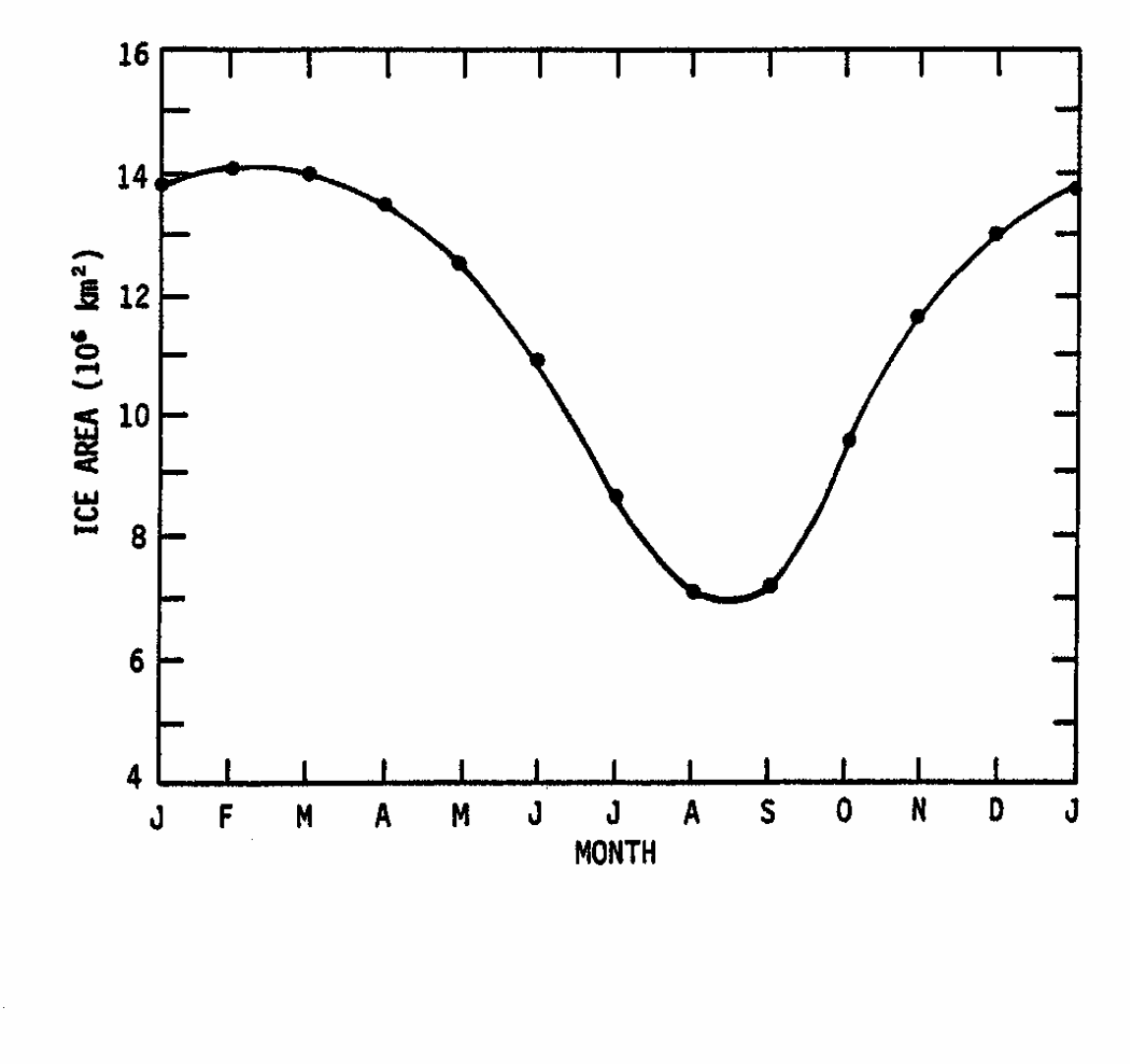

Figure 6. Typical annual Northern Hemisphere sea ice extent. From Walsh and Johnson, 1979.

Understanding both seasonal and interannual seesaw effects are important for the United States Navy when attempting to forecast ice thickness and extent. To do this, the Navy uses the Polar Ice Prediction System (PIPS), (Preller *et al.,* 2002). This model makes use of real time and climatological atmospheric data, the Cox Ocean Model, and the Hibler Ice model to produce a forecast for ice approximately five days in the future (Preller *et al.,* 2002) (Fig.7). One problem with PIPS documented by Preller *et al.* (2002) is that it often over-predicts ice in the Barents Sea and under-predicts ice in the Labrador Sea. This over-prediction of ice may be attributed to the poor resolution of smaller advective processes like currents or river run-off (Mellor and Hakkinen, 1994). Another possibility for the discrepancies in prediction is that the model does not resolve the heat fluxes in these regions as accurately as needed. Specifically, the Labrador Sea has heat fluxes and deep mixed layers more consistent with the Antarctic region than other Arctic seas, and so the vertical processes of this sea generate greater amounts of ice than predicted (Guest, personal communication).

C. LEADS AND POLYNYAS

Leads and polynyas are both areas of open water where ice would have been predicted given the climatology of the surface forcing by the atmosphere. There are two types of polynyas enumerated by Smith *et al.* (1990); the first is a "latent heat" polynya that is maintained by horizontal advective heating processes attributable to wind and currents. The second is a "sensible heat" polynya that is created from vertical convective heating from the ocean. In either case the net heat flux into that area is sufficient to inhibit ice formation. As this research is focused primarily on vertical effects, the "sensible heat" polynya is of greatest interest. Smith *et al.* (1990) describe leads as open channels within the ice that are created by a divergence in the ice flow. Leads are also of interest especially when considering that ocean dynamics and heating from below may develop weaknesses in the ice. When the weaker ice is put under stress from wind or surrounding ice it diverges into open water channels.

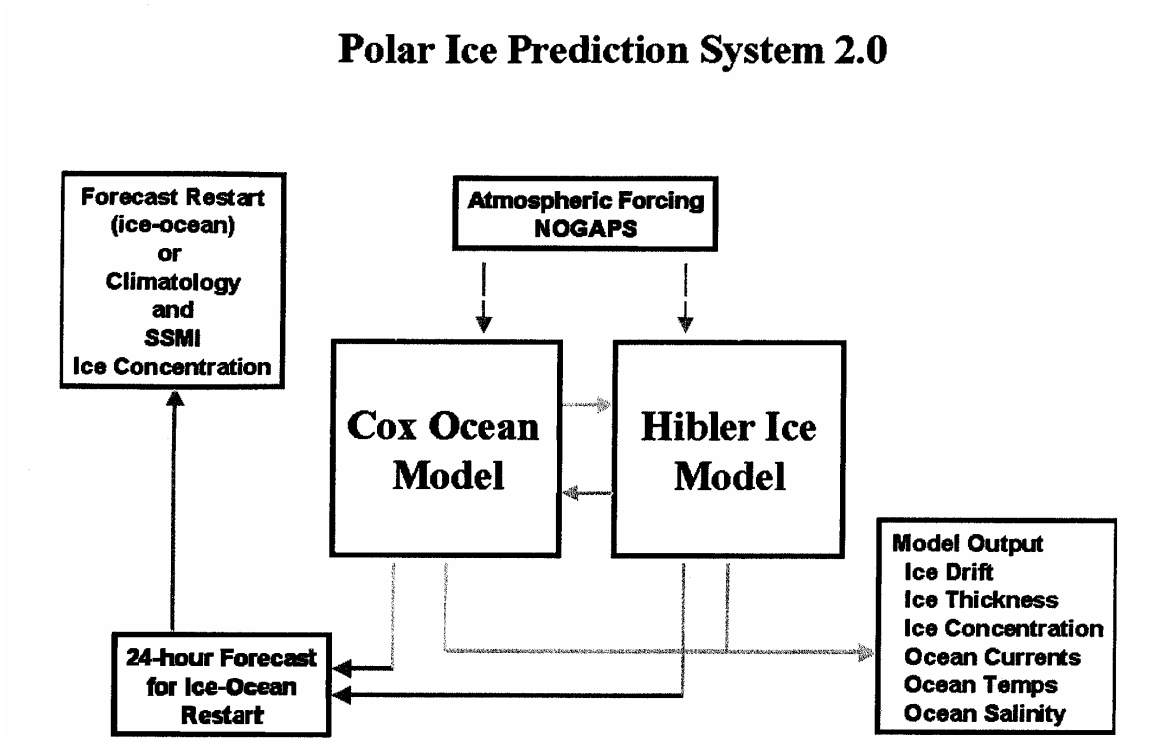

Figure 7. U.S. Navy PIPS Model. From Preller *et al.,* 2002.

While lead location does have a stochastic nature, polynyas often recur in the same location with some periodicity. However, it is important to note, as Smith *et al.* (1990) does, that the Weddell Sea sensible heat polynya disappeared in the 1980's after having appeared regularly in the late 1970's. This indicates the strong dependence of open water formation on the dynamics occurring beneath the surface and suggests that climatological conditions, while important, are not the sole causes. Similarly, the seasonal nature of the heat flux, with greater heat flux out of the water in winter, is no assurance of ice formation; nor does summer warming of the water column guarantee complete ice melting.

In regards to the Weddell Sea in Antarctica, Martinson *et al.* (1981) assert that the Weddell Polynya cannot be created by wind forcing or atmospheric effects alone since the low-pressure system required to create it would not survive long enough in this environment. Instead, they postulate that some type of preconditioning occurs to raise the pycnocline from below the mixed layer. Martinson *et al.* (1981) offer several possibilities for the source of the preconditioning including both topography and mean flow spin-up. The preconditioning, whatever its source, coupled with salt rejection at the surface during freezing causes a layer of cold fresh water above a raised portion of warm salty water from below. When the density of the cold fresh water surpasses that of the warm salty water the column can overturn leaving warm salty water at the surface. In this way freezing of ice initiates a negative feedback where the end result is ice melting from the heat of the newly raised water just below the ice at the surface of the water column. Because of density driven overturning Martinson *et al.* (1981) contend that the temperature and salinity profiles of both the pycnocline beneath the mixed layer and the mixed layer itself are vital for determining the formation of the Weddell Polynya. It is of interest to note, as well, that although no conclusions are made in regards to the effects of topography, Martinson *et al.* (1981) do speculate that the polynya is subject to the circulation of the Weddell gyre and appears to cycle from the east to the west with the mean flow. Furthermore, they suggest evidence that the polynya moves to an extreme westward location before it is recreated at its extreme eastern-most point (Martinson *et al.,* 1981).

THIS PAGE INTENTIONALLY LEFT BLANK

III. THEORY

A. PREVIOUS STUDIES

Recognizing the importance of atmospheric conditions and seasonal variations is necessary for predicting ice freezing and melting. Similarly, as in the case of the Weddell Polynya and mentioned by Martinson *et al.* (1981), the circulation patterns, both surface and subsurface, and/or bathymetry may aid or precondition melting or freezing effects. However, since low or high pressure systems and their accompanying winds come and go at varying time scales, and bathymetry remains relatively constant within a region, the physics of the water column is the most significant component of sustained surface freezing and melting. More specifically, the coupled thermodynamics and dynamics that together mix water vertically upwards and downwards contribute the most to ice freezing or melting. Lemke *et al.* (1990) explain the importance of this coupling by suggesting that a situation may develop where ice melts due to thermodynamic effects creating an area of no ice, but then freezes again, almost immediately, due to water movement at the surface. This argument highlights the need for the source of the heat, in addition to the heat it provides, to be brought to the surface for a sustained no-ice area to exist in the polar climate.

Hakkinen (1987) explains the thermodynamics and dynamics necessary to bring heat to the surface and sustain it using a two-layer model. The two layers suggested by Hakkinen (1987) are a cold fresh surface layer and a warm salty bottom layer that is at rest. As described by Kraus and Turner (1967) the heat and salinity fluxes between these two layers are dependent upon the difference between the temperature and salinity profiles of each layer respectively. Hakkinen (1987) investigates the vertical transfer of heat on the mesoscale. Specifically, she focuses on entrainment of warm salty water from the lower layer up into the surface layer at the ice edge in the marginal ice zone (Hakkinen, 1987). Her one-dimensional model suggests that entrainment has an inverse dependence on density; as the depth of the mixed layer increases entrainment decreases, thereby ensuring that the mixed layer does not deepen infinitely (Hakkinen, 1987).

Dynamically, Hakkinen (1987) relies on strong winds blown across the surface to create drag on the water column. This drag, which is three times as great when there is ice at the surface as when there is no ice present, creates strong Ekman transport (Hakkinen, 1987). Not surprisingly, the greater the drag the greater the Ekman transport, and so Ekman transport is greatest under the ice (Hakkinen, 1987). In order to quantify the drag Hakkinen (1987) defines a fractional calculation of ice compactness, A. Hakkinen's (1987) preconditioning, as termed by Martinson *et al.* (1981) for the priming of upcoming interaction between the two layers, comes from the stronger Ekman transport down beneath the ice that leads to increased upwelling at the ice edge. Through this mechanism upwelling assists entrainment in keeping warmer and more saline water at the surface and keeps the area free of ice (Hakkinen, 1987).

Lemke *et al.* (1990) similarly use a one-dimensional two-layer model consistent with Kraus and Turner (1967) to explain sustained heat at the surface. Like Hakkinen, Lemke *et al.* (1990) is concerned with the momentum balance between the atmosphere, ice, and water column. Lemke *et al.* (1990) combines the equations of motion, ice compactness and coverage, the nonlinear viscous-plate constitutive law from Hibler (1979), and atmospheric forcing to explain vertical movement of heat. Lemke *et al.* (1990) also find that the greatest vertical heat flux in the Weddell Sea is at the ice edge.

Unlike Hakkinen (1987), however, Lemke *et al.* (1990) focus less on atmospheric forces like wind and more on the entrainment velocity as the mechanism for heating at the surface. In other words, the overall oceanic heat flux is dependent on the entrainment velocity (Lemke *et al.*, 1990). This means that whether ice melts or freezes it is directly dependent on the entrainment velocity. According to Lemke *et al.* (1990) positive entrainment brings heat to the surface and melts the ice, entrainment less than zero extends the mixed layer to the depth of the water column, and entrainment equal to zero, setting the mixed layer depth equal to the Monin-Obukhov length, occurs when the two layers are thermodynamically independent of one another. Lemke *et al.* (1990) formulate the entrainment values to be dependent upon the equation of state, and thereby effectively emphasize the role of the temperature and salinity expansion coefficients. Furthermore, the inclusion of the equation of state underscores the importance of changes in both

temperature and salinity between the abyss and the mixed layer for vertical heat exchange (Lemke *et al.,* 1990).

B. THERMOBARICITY

Thermobaricity is an important process to include when attempting to model or understand the complete physics of the mixed layer. It is defined as the combined dependence of seawater thermal expansion on temperature and pressure (McDougall, 1984). The work done by Lemke *et al.* (1990) lays the groundwork for the significance of thermobaricity. It is important because it magnifies the buoyancy flux associated with mixed layer convection (Garwood, 1991). If thermobaricity is included in the equation of state the thermal expansion coefficient, α, is no longer a constant, but is instead a function of both temperature and depth. This means that entrainment is not only a function of the differences in temperature and salinity between the abyss and mixed layer, but is also a function of the depth and temperature of the abyss-mixed layer boundary. The physical result of the inclusion of thermobaricity is consistent with Lemke *et al.* (1990); when entrained heat from below is greater than the heat leaving the water column, the mixed layer warms and any existing ice begins to melt. Similarly, if entrained heat is less than the heat leaving the column the mixed layer cools and freezing occurs at the surface. However, the magnitude of the entrainment could be very different with the inclusion of thermobaricity, under certain conditions, resulting in either freezing or melting when Lemke *et al.* (1990) predict the opposite.

Garwood *et al.* (1994) shows the necessity of understanding thermobaricity and the importance of being able to model it. He enumerates four different scenarios where thermobaric effects have implications in polar modeling.

1) Mixed-layer turbulent kinetic energy (TKE) may be increased several-fold by the thermobaric amplification of the buoyancy flux (Garwood, 1991). This phenomenon is not significant at temperate and low latitudes, but it becomes large for polar sea mixed layers. It cannot be neglected for realistic air-sea ice interactions. Large eddy simulation (LES) verifies its importance in increasing entrainment. However, commonly used parameterizations of ocean mixing, including second-order closure of Mellor and

Yamada (1982) and k-profile parameterization (KPP) (Large et al., 1994), do not yet include this physics.

2) Buoyancy is not conserved in coastal subduction. Although buoyancy is well conserved in vertical advection of water masses at lower latitudes, it is not a conservative property in the polar seas. This is especially important for vertical circulation that is enhanced on shelf slopes. Here it becomes a severe limitation for layered models that presume a constant potential density for each layer (Garwood and Isakari, 1993; Jiang and Garwood, 1995, 1996, 1998).

3) "Thermobaric stability" is an increase in the hydrostatic stability of seawater having positive spiciness and nearly density-compensating T-S structure. It causes spicy warmer and saltier parcels to resist vertical mixing because of a newly recognized thermobaric component to the buoyancy frequency. This added component depends upon the thermobaric depth H_α. This phenomenon enables internal gravity waves without vertical buoyancy gradient (Garwood, 2002), and it helps explain lateral intrusion of filaments of spicy water across T-S frontal zones. Furthermore, the theory predicts reduced stability for cold and fresh filaments with negative spiciness. This process is potentially important in enhancing shoreward transport but reducing the flux of suspended and dissolved material from the shelf into the Arctic interior.

4) A critical mixed-layer depth h_{cr} for maintenance of open water and sensible heat polynyas (Smith et al., 1990) under freezing atmospheric temperatures is predicted because of thermobaricity (Garwood, 2001). Whenever the mixed layer depth exceeds a critical depth, the entrainment heat flux w_e will exceed the surface heat loss to the atmosphere Q_0, resulting in ice melting regardless of the rate of heat loss to the atmosphere from the ice-mixed layer system. This is a positive feedback mechanism for warming the surface layer, limiting ice formation, and cooling the ocean interior. It undoubtedly plays a role in establishing the extent and geographic evolution of the marginal ice zone, and in the maintenance of polynyas and their entrainment of nutrient-rich water into the surface layer.

C. FUNDAMENTAL EQUATIONS

Since Kraus and Turner (1967) first modeled the mixed layer, oceanographers have worked to understand the role of turbulence in mixed layer dynamics. Their focus was limited to the temperate oceans and the role of air-sea interactions on turbulence. Independently, since Hibler (1979), polar oceanographers have proposed and advanced models for ice mechanics, with cursory attention to mixed layer turbulence. Recognizing the need to consider mixed layer dynamics under the ice, Lemke *et al.* (1990) and Hakkinen (1987) included linear formulations for entrainment into their coupled ice-ocean numerical models. However, Garwood (1991) showed that the equation of state's nonlinear properties needed to be included when considering turbulent mixing in the cold water of the polar seas.

The physical processes of the coupled system depend heavily on the vertical entrainment of warmer, saltier, and denser water from below. Normally in the lower latitudes the denser water from below is both colder and saltier than the water above it, but in the high latitudes where salinity is the dominate determinate of density, it is the warm and saline water that makes up the high density water from below. Entrainment, or the rate of deepening of the mixed layer, is important for two primary reasons. First, entrainment is needed to calculate both the temperature and salinity fluxes that make up the buoyancy flux. Second, when ice is present at the surface, entrained water may heat the ice layer directly without heating the mixed layer significantly, and so ice thickness is directly dependent on the entrainment.

Prediction of polar sea mixed layer dynamics and thermodynamics is dependent upon the same physics that governs all water parcel motion: the Reynolds equations for the mean momentum, which are derived from the Navier-Stokes equations,

$$\overline{u}_t + \overline{u}\overline{u}_x + \overline{v}\overline{u}_y + \overline{w}\overline{u}_z = -\frac{\overline{p}_x}{\rho} + f\overline{v} - f_y\overline{w} - \left(\overline{u'u'}\right)_x - \left(\overline{u'v'}\right)_y - \left(\overline{u'w'}\right)_z + \upsilon\left(\overline{u}_{xx} + \overline{u}_{yy} + \overline{u}_{zz}\right) \quad (1)$$

$$\overline{u}_t + \overline{u}\overline{u}_x + \overline{v}\overline{u}_y + \overline{w}\overline{u}_z = -\frac{\overline{p}_x}{\rho} + f\overline{v} - f_y\overline{w} - \left(\overline{u'u'}\right)_x - \left(\overline{u'v'}\right)_y - \left(\overline{u'w'}\right)_z + \upsilon\left(\overline{u}_{xx} + \overline{u}_{yy} + \overline{u}_{zz}\right) \quad (2)$$

$$\overline{w}_t + \overline{u}\overline{w}_x + \overline{v}\overline{w}_y + \overline{w}\overline{w}_z = -\frac{\overline{p}_z}{\rho} + f_y\overline{u} - g - \left(\overline{u'w'}\right)_x - \left(\overline{v'w'}\right)_y - \left(\overline{w'w'}\right)_z + \upsilon\left(\overline{w}_{xx} + \overline{w}_{yy} + \overline{w}_{zz}\right) \quad (3)$$

the continuity equation,

$$u_x + v_y + w_z = 0 \tag{4}$$

the heat and salt equations where the Reynolds decomposition is also applied with $T = \overline{T} + T', S = \overline{S} + S'$, averaged, and put into flux form as,

$$\frac{D\overline{T}}{Dt} = \overline{T}_t + \overline{u}\overline{T}_x + \overline{v}\overline{T}_y + \overline{w}\overline{T}_z = -\left(\overline{T'u'}\right)_x - \left(\overline{T'v'}\right)_y - \left(\overline{T'w'}\right)_z + \kappa_T\left(\overline{T}_{xx} + \overline{T}_{yy} + \overline{T}_{zz}\right) \tag{5}$$

$$\frac{D\overline{S}}{Dt} = \overline{S}_t + \overline{u}\overline{S}_x + \overline{v}\overline{S}_y + \overline{w}\overline{S}_z = -\left(\overline{S'u'}\right)_x - \left(\overline{S'v'}\right)_y - \left(\overline{S'w'}\right)_z + \kappa_S\left(\overline{S}_{xx} + \overline{S}_{yy} + \overline{S}_{zz}\right) \tag{6}$$

and the equation of state,

$$\rho = \rho_o[1 - \alpha(T - T_o) + \beta(S - S_o)] \tag{7}$$

Prediction of the turbulent fluxes, and entrainment in particular, is based upon the Turbulent Kinetic Energy (TKE) equation, which is also derived from the Navier-Stokes equations,

$$\begin{aligned} &\frac{\partial}{\partial t}\left(\frac{\overline{u'^2} + \overline{v'^2} + \overline{w'^2}}{2}\right) = \\ &-\left[\overline{u'w'}\frac{\partial\overline{u}}{\partial z} + \overline{v'w'}\frac{\partial\overline{v}}{\partial z}\right] + \overline{b'w'} - \frac{\partial}{\partial z}\left[\overline{w'\left(\frac{u'^2 + v'^2 + w'^2}{2} + \frac{p}{\rho_0}\right)}\right] - \varepsilon \approx 0 \end{aligned} \tag{8}$$

This equation calculates the energy available to do work created from shear production, $\left[\overline{u'w'}\frac{\partial\overline{u}}{\partial z} + \overline{v'w'}\frac{\partial\overline{v}}{\partial z}\right]$, and the vertical fluxes of temperature and salinity that make up the vertical buoyancy flux, $\overline{b'w'} = \alpha g\overline{T'w'} - \beta g\overline{S'w'}$. The four terms to the right of the equals sign in the TKE equation are, from left to right, as follows: the shear production of horizontal turbulent kinetic energy, the production or damping of vertical turbulent kinetic energy by buoyancy forces, redistribution, and dissipation. These terms apply to the mixed layer whether or not ice is present at the surface. The shear production term is always non-negative, and horizontal turbulent kinetic energy is a direct result of the wind stress at the surface and produces "forced convection." Vertical turbulent kinetic energy is produced whenever the buoyancy flux is positive due to negative salinity flux and/or positive temperature flux. Positive buoyancy flux results in "free convection." Buoyancy flux will always be negative at the bottom of the mixed layer, where the turbulent kinetic energy is used to entrain the underlying heavier water into the mixed

layer. Redistribution moves turbulent kinetic energy vertically within the mixed layer. Dissipation converts turbulent kinetic energy to heat, and is always a loss term.

To solve for the entrainment it is necessary to solve for the vertical integral of the TKE equation. If equation (8) is vertically integrated over the mixed layer, the entrainment velocity may be calculated in terms of the stratification (ΔT and ΔS), mixed layer depth, h, and the forcing velocity scales (u_* and w_*), which are defined below.

$$w_e = \frac{c_1 u_*^3 + c_2 w_*^3}{\alpha_o g h \Delta T \left(1 + \frac{h}{H_\alpha}\right) - \beta_o g h \Delta S} \tag{9}$$

The resulting equation (9) shows that all of the available energy to do work, or stirring in this case, is provided from either forced convection from wind or ice forcing, or from the free convection from within the water column. Forced convection,

$$c_1 u_*^3 = \int_{-h}^{0} -\left[\overline{u'w'}\frac{\partial \bar{u}}{\partial z} + \overline{v'w'}\frac{\partial \bar{v}}{\partial z} + \varepsilon\right] dz \tag{10}$$

originates in the atmosphere and quantifies the turbulence created from wind blowing across the surface or across ice at the surface. Free convection, or positive $c_2 w_*^3$, is the vertical integral of the buoyancy flux over the mixed layer,

$$c_2 w_*^3 = \int_{-h}^{0} \overline{b'w'} dz \tag{11}$$

As can be seen in the equation for entrainment (9) the equation of state (7) has a significant influence on the buoyancy flux and magnitude of free convection (11). It should be mentioned that the term "free convection" only applies when w_*^3 is positive. If w_*^3 is negative the integrated buoyancy flux dampens the turbulence. Appropriately, this situation is referred to as "buoyant damping." The value of w_*^3 can be positive under the ice if freezing is occurring at the surface. If melting is occurring w_*^3 is negative regardless of the Q_0 value. In the ice-free system w_*^3 is positive when the net heat flux is positive (out of the system). When the net heat flux is negative, or into the ice-free system (summer conditions), w_*^3 is negative as well.

The net effect of dissipation is absorbed by the coefficients, c_1 and c_2. For this work the coefficients c_1 and c_2 are considered tunable constants. Kraus and Turner (1967) assumed c_1 and c_2 to be constant. First Gill and Turner (1976), and later Garwood (1977) showed that both c_1 and c_2 vary with mixed layer stability. However, c_1 and c_2 may be considered constant for slowly changing surface forcing conditions, which are assumed in this study. The parameter H_α is the "thermobaric depth" (Garwood, 1991) for which increased pressure doubles the thermal expansion relative to the surface value, α_0, and will be discussed further in the following paragraphs.

The buoyancy flux is a function of both the potential temperature flux and the salinity flux. The vertical integral of the buoyancy flux,

$$\int_{-h}^{0} \overline{b'w'}(z)\,dz = \int_{-h}^{0} \left(\overline{b'w_\theta'} + \overline{b'w_S'}\right) dz$$

shows this dual dependence. Breaking buoyancy flux into these two components and solving demonstrates how each of the fluxes is dependent on vertical entrainment. The two components are,

$$(1)\ \overline{b'w_\theta'} = \alpha g\left[\overline{\theta'w'}_0\left(1+\frac{z}{h}\right) - \overline{\theta'w'}_{-h}\left(\frac{z}{h}\right)\right]$$

$$\text{where } \alpha = \alpha_o\left(1-\frac{z}{H_\alpha}\right)$$

$$(2)\ \overline{b'w_S'} = \beta_o g\left[\overline{S'w'}_0\left(1+\frac{z}{h}\right) - \overline{S'w'}_{-h}\left(\frac{z}{h}\right)\right]$$

The vertical fluxes are related to entrainment by,

$$(1)\ \overline{\theta'w'}_{-h} = -\Delta\theta w_e$$

$$(2)\ \overline{S'w'}_{-h} = -\Delta S w_e$$

where $\Delta\theta$ and ΔS are the jumps in potential temperature and salinity at the base of the mixed layer. The potential temperature (θ) and the *in situ* temperature (T) are assumed to be equal in this study, with negligible error. Taking the vertical integral of each

component yields w_*^3, the vertical integral of the buoyancy flux, and its dependence on the vertical entrainment velocity:

$$w_*^3 = -\left[\beta_o g h * \frac{S - S_i}{2}\right] * mf - \left[\alpha_o g h * \left(1 + \frac{h}{H_\alpha}\right) * \Delta T - \frac{\beta_o g h * \Delta S}{2}\right] * w_e \qquad (12)$$

The temperature and salinity fluxes follow directly from the temperature and salinity profiles as well as the net heat flux into or out of the water column (Fig. 8). Temperature and salinity profiles in the high latitudes are quite unique, especially with the presence of ice (Fig 9). Assuming ice coverage, the water just below the ice will be warmer than the ice; if it were not warmer it too would be frozen. Consequently, the water just below the ice is warmer than the freezing point and usually continues to get warmer with depth. Similarly, since ice rejects salt when it freezes, the ice will have a much lower salinity than the water beneath it. Salinity usually continues to increase with depth. Recalling that salinity dominates over temperature in the high latitudes, these profiles create a stable density structure.

When there is ice coverage all of the entrainment works directly to heat the ice layer and does not heat the mixed layer significantly. When this occurs the ice begins to melt and so the vertical entrainment velocity affects ice thickness (h_i) as well:

$$-\frac{dh_i}{dt} = +(mf) = \frac{-Q_o}{\rho_i L_f} - \frac{\rho c_p * \Delta T * w_e}{\rho_i L_f} \qquad (13)$$

where mf is the melting-freezing term, $\rho_i L_f$ quantifies the latent heat of fusion, and ρc_p is the water density times the heat capacity. When the entrainment heat flux exceeds the upward flux of heat and radiation at the ice surface (Q_0), then the ice will melt making $\frac{dh_i}{dt} < 0$. Conversely, when the entrainment is weaker than the surface heat flux ice will freeze making $\frac{dh_i}{dt} > 0$.

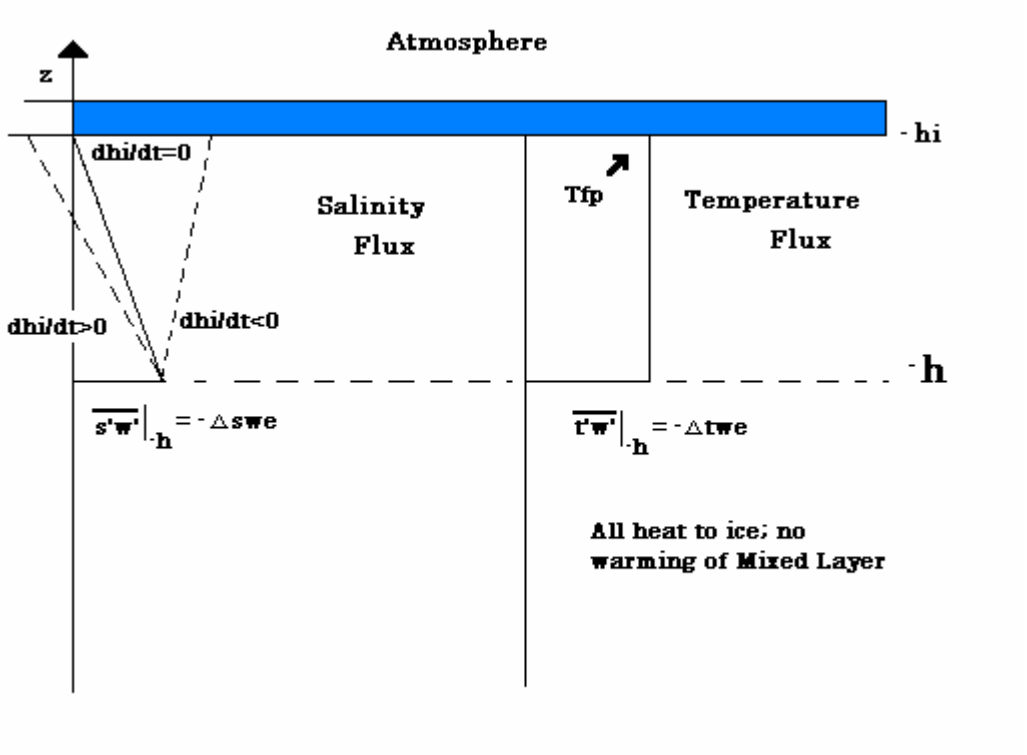

Figure 8. Representative temperature and salinity flux profiles for the high latitude regions.

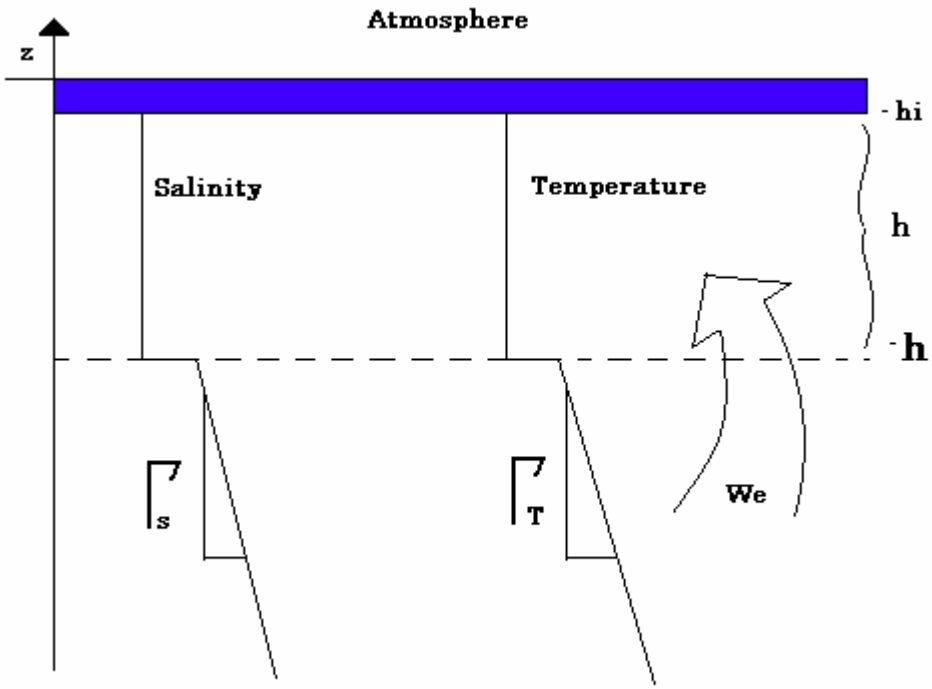

Figure 9. Representative salinity and temperature profiles for the high latitude regions.

In this way vertical entrainment simultaneously affects both free convection and the ice thickness. Therefore, to solve for entrainment requires solving three simultaneous equations, one for free convection, w_*^3, one for change in ice thickness, $-\frac{dh_i}{dt}$, and one for vertical entrainment velocity itself, w_e.

Accuracy of the calculation of buoyancy flux is improved by considering thermobaric enhancement of entrainment. This occurs when the thermal expansion coefficient, α, is no longer treated as a constant but is allowed to vary with both temperature and depth. Consequently, the equations for both vertical entrainment velocity and free convection contain the term H_α, the "thermobaric depth", as well as the surface term for the thermal expansion coefficient, α_0. The inclusion of thermobaric depth can lead to a magnified entrainment rate, increased buoyancy, and more efficient stirring of the mixed layer through free convection. It is through this process that heating of the ice can occur more quickly and with greater intensity. Prolonged enhanced entrainment in a region can lead to a polynya, where the ice has been melted away completely and the entrainment works to warm the mixed layer to greater depth.

Under certain situations free convection can be turned off, $c_1 w_*^3 = 0$, or even be made negative. As discussed previously, when this term is negative it is no longer called free convection but is instead called buoyant damping. This situation occurs when the entrainment shuts down or is very weak. Entrainment, however, can never be made negative since un-stirring, or directly reversing completed work cannot be achieved. If free convection were to shut down, forced convection could dominate and wind stirring of the mixed layer could result. When this happens the mixed layer could shallow to the Obukhov Length (L), and a step would be noticed in the density profile consistent with summer shallowing conditions. It is important to note that for the model created in association with this work, circumstances leading to a negative sum of the free and forced convection will not be processed accurately.

D. MODEL

A one-dimensional model consisting of a system of ordinary differential equations was solved as an initial-value problem numerically to examine the interaction between the mixed layer and ice at the surface. The model was designed this way so that particular attention could be paid to the importance of thermobaricity as well as the strength of various forcing terms and initial conditions. Additionally, this model was built with the idea that it could be used directly or as the precursor for a model that will be able to fit with current ice prediction models. Specifically, the model should ultimately work in conjunction with the Hibler Ice Model so that the United States Navy can use it operationally in systems like PIPS (Fig .7). The end goal for the future model is simple: forecasts for ice formation, thickness, and extent must all improve over today's model output. For example, the ice thickness in the Greenland Sea, which is currently often poorly predicted, may be more accurately represented. The model must be robust enough to generate ice-free areas like polynyas or ice covered regions given any initial ice condition and representative atmospheric conditions. In other words, given realistic forcing and initial conditions, the model should predict a polynya in an area that is ice covered or freezing in a polynya. Matlab's C++ was chosen as the programming language for this model because of its matrix, differential equation, and graphical capabilities, as well as its ability to perform large calculations with minimal user effort.

1. Model Equations Summarized

a. Coupled Mixed Layer-Ice System Equations

The system of eight equations is derived by vertically integrating the budgets for enthalpy (heat)(5), momentum (2)(3), salinity (6) and TKE (8) between the ice surface and the base of the turbulent mixed layer. Drag (momentum flux) and heat flux between the ice and mixed layer are calculated with bulk aerodynamic scaling laws, with the temperature of the ice-water contact assumed to be at the freezing point, T_{fp}. Entrainment fluxes of heat, salinity and momentum are derived from integrating the respective conservation laws (2, 3, 5, and 6) across the entrainment zone discontinuity (Garwood, 1977).

Mixed Layer Depth:

$$\frac{dh}{dt} = w_e = \left\{ c_1 u_*^3 - c_2 \left[\alpha g \frac{Q_0}{\rho c_p} + \beta g (mf)\left(\langle S \rangle - S_i \right) \right] \right\} / \{ \alpha g \Delta T - \beta g \Delta S \} \quad (14)$$

Mixed-Layer Temperature:

$$\frac{d\langle T \rangle}{dt} = \frac{Q_0}{\rho c_p h} - \frac{\Delta T}{h} w_e \quad (15)$$

Mixed-Layer Salinity:

$$\frac{d\langle S \rangle}{dt} = -(mf) \frac{\left(\langle S \rangle - S_i \right)}{h} - \frac{\Delta S}{h} w_e \quad (16)$$

Ice thickness:

$$\frac{dh_i}{dt} = -(mf) = \frac{Q_0 - \rho c_p \overline{T'w'}\Big|_{-h}}{\rho_i L_f} \quad (17)$$

Mixed-Layer Currents:

$$\frac{d\langle u \rangle}{dt} = \frac{\tau_{x_i}}{\rho h} + f\langle v \rangle - \frac{\langle u \rangle}{\tau} - \frac{\Delta u}{h} w_e \quad (18)$$

$$\frac{d\langle v \rangle}{dt} = \frac{\tau_{y_i}}{\rho h} - f\langle u \rangle - \frac{\langle v \rangle}{\tau} - \frac{\Delta v}{h} w_e \quad (19)$$

Ice velocity:

$$\frac{du_i}{dt} = \left(\frac{\tau_{x_o} - \tau_{x_i}}{\rho h_i} \right) + f v_i \quad (20)$$

$$\frac{dv_i}{dt} = \left(\frac{\tau_{y_o} - \tau_{y_i}}{\rho h_i} \right) - f u_i \quad (21)$$

Momentum and Heat Flux Between Ice and Mixed Layer:

$$\tau_{xi} = \rho C_D (u_i - u) \sqrt{(u_i - u)^2 + (v_i - v)^2} \quad (22)$$

$$\tau_{yi} = \rho C_D (v_i - v) \sqrt{(u_i - u)^2 + (v_i - v)^2} \quad (23)$$

$$\overline{T'w'}\Big|_{-h} = \frac{C_T}{\sqrt{C_D}} u^* \left[\langle T \rangle - T_{fp} \right] \qquad (24)$$

$$u_*^3 = \left(\tau_i / \rho \right)^{3/2}$$

$$\text{where: } \tau_i = \sqrt{\left(\tau_x \right)^2 + \left(\tau_y \right)^2} \qquad (25)$$

2. Numerical Methods

Matlab is a programming language that can perform large calculations and provide graphical representation of data through the manipulation of matrices and execution of user produced or existing functions. Its ability to quickly and accurately perform complicated and or lengthy computations make it an attractive tool for ocean modeling.

a. Use of Stiff Solver

ODE23s is a Matlab function that solves ordinary differential equations using a stiff solver. The use of ODE23s allowed for the tracking and graphing of many different oceanographic parameters as the program stepped forward in time. Specifically, it kept track of and depicted how both the mixed layer depth and ice thickness increased or decreased given the initial and forcing conditions. The program ODE23s was chosen over other Matlab differential equation solvers because of its ability to solve stiff differential equations. A way of solving this type of equation became necessary when approaching or crossing into the ice-free regime, where intermediate solutions change rapidly, but the final solution is found on a longer time scale (Shampine, 1994). Not using a stiff solver would mean allowing for the time step to decrease so that every intermediate solution could be calculated. This ability was not necessary since the final solution was the solution of interest. To numerically solve these types of equations Matlab employs the Runge-Kutta formula or, in the case of ODE23s, a modified Rosenbrock formula that is more efficient (Math Works, 2002). Additionally, because of the computational power and time benefits of this program, it was verified that treating the water column as three slabs was a robust method for the desired modeling. This was proven graphically by showing that the total of the velocities of the ice layer slab and

mixed layer slab, individually, were equal in value to the velocity of a combined ice-mixed layer slab.

IV. SENSITIVITY STUDIES

The following sensitivity studies simulated Weddell Sea winter conditions. Akitomo (1999) first applied Garwood *et al.* (1994) thermobaric instabilities to the Weddell Sea, but without the ice-mixed layer feedback model used here. This was done because there is greater interaction between temperature and salinity in this region and at this time. For each simulation one of the forcing conditions, net heat flux (Q_0) or wind speed, was held constant while the other was allowed to vary. Similarly, the initial conditions were varied for the simulations. Two different depths of the mixed layer were chosen to examine the effects of the ratio between mixed layer depth and thermobaric depth. These depths were 100 m for a moderately deep mixed layer and 1000 m for a deep mixed layer. The effects of changing the ratio of thermal stratification to salinity stratification, $\alpha_0 g\Delta T$ to $\beta_0 g\Delta S$, on ice melting and freezing at the surface were examined.

It should be noted that the program allows for the ratio of $\alpha_0 g\Delta T$ to $\beta_0 g\Delta S$ to change with changing temperature and salinity values. If these values were instead prescribed, accuracy would be lost since it would effectively not allow for any storage of heat or salt in the mixed layer when ice is present at the surface. Furthermore, any warm salty water entrained would not change the mixed layer temperature and salinity values. Equations from the previous chapter demonstrate how important the temperature and salinity fluxes within the mixed layer are to the free convection and total turbulent kinetic energy of the system. Not allowing for these fluxes is the equivalent of neglecting physical processes essential to the coupled ice-mixed layer system. Instead, by allowing for this change in the ratio, the vertical integral of the buoyancy flux can be accurately calculated.

In all simulations the initial ice thickness is 10 cm; the initial temperature is the temperature of the freezing point at the surface, -1.66 Celsius; the initial salinity value is 34.52 parts per thousand; and the thermobaric depth is 93.6 m. Since both 100 m and 1000 m mixed layers are deeper than the thermobaric depth, thermobaricity is expected to

enhance the entrainment of warmer and saltier water from below. Each case is run for ten days, or $8.64x10^5$ seconds.

A. MIXED LAYER DEPTH EQUAL TO 100 METERS

For the first simulation at h=100 m, the ratio of $\alpha_0 g\Delta T$ to $\beta_0 g\Delta S$ equaled 0.45 for the surface temperature and salinity values. The total heat flux was a constant 0.001 cal/cm^{2}s upward and out of the coupled system. The wind speed was allowed to vary from 400 cm/s to 1600 cm/s in 400 cm/s increments. The results show that for each wind speed positive entrainment deepens the mixed layer (Fig. 10). The weakest wind, 400 cm/s, produced the least amount of mixed layer deepening. The resultant entrainment was not strong enough to melt ice at the surface and instead fostered ice growth.

The mixed layer salinity increases for the 400 cm/s wind as freezing occurs and salt is rejected from the ice. The corresponding mixed layer temperature warms until it comes into equilibrium. Once the temperature equilibrium is reached, the rate of salinity increase, ice growth, and mixed layer deepening all become constant.

The higher wind values of 800 cm/s, 1200 cm/s, and 1600 cm/s each produced strong enough entrainment to melt the ice and deepen the mixed layer, with the 1600 cm/s wind having the strongest melting rate. Similarly, the 1600 cm/s case had the largest decrease in salinity associated with the melting of the ice and injection of fresh water into the mixed layer. Correspondingly, the mixed layer temperature warmed the most significantly immediately before eventually approaching equilibrium. It should be noted that the 1600 cm/s plots do not extend to the full ten days like the other wind speeds. This is due to the strong entrainment that occurs and the ill-defined matrix that results when trying to continue to solve for the entrainment and w_*^3 terms simultaneously.

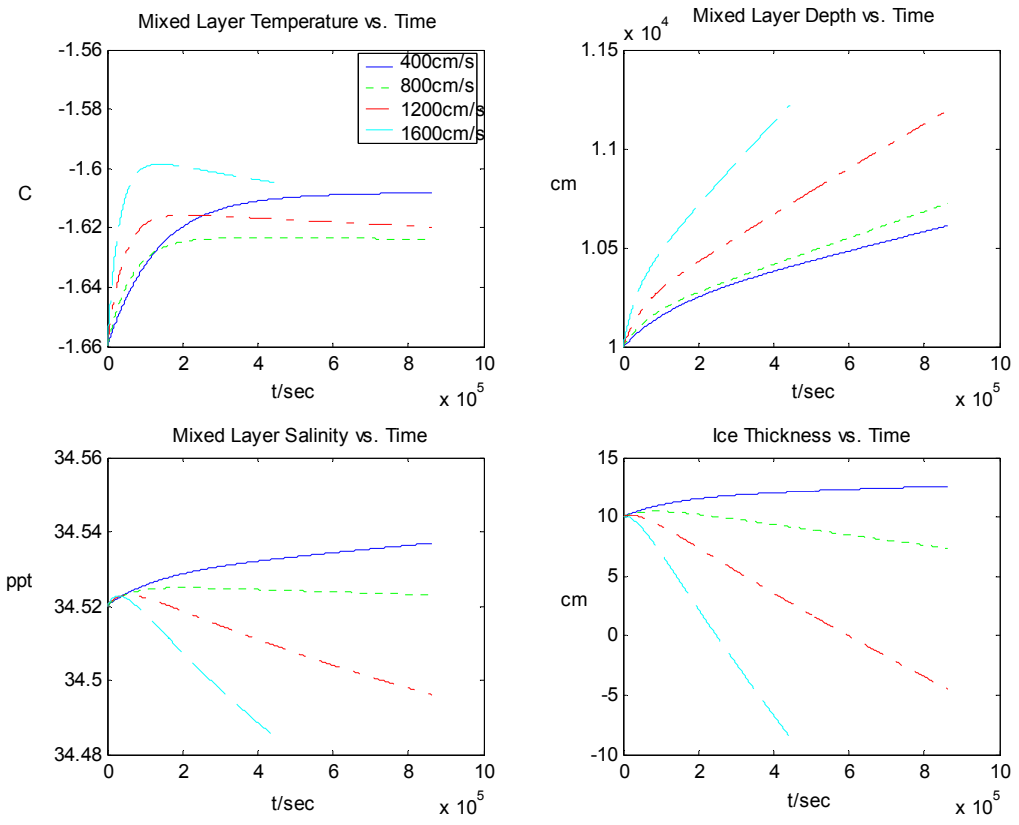

Figure 10. Simulation #1: Sensitivity study for varying winds with h =100 m, Q_0=0.0010 cal/cm^{2}s, and ratio of $\alpha_0 g\Delta T$ to $\beta_0 g\Delta S$ equal to 0.45. Wind speed changes from 400 cm/s to 1600 cm/s in 400 cm/s intervals.

Winds of 1200 cm/s and 1600 cm/s are capable of melting away the ice completely; however, once the ice is melted away the model shows negative ice thickness at approximately 2.3 days ($2.0x10^5$ sec) and 6.9 days ($6.0x10^5$ sec) respectively. This is an unrealistic depiction of the true physical process; there is no such thing as negative ice. Similarly, an unrealistic decrease in salinity values is achieved for these wind speeds at the same points in time. The salinity values are unrealistic because once the ice has melted away there is no other source of fresh water to continue to decrease the salinity of the mixed layer. Future versions of the model need to be able to melt away the ice, remain ice-free without predicting negative ice, and then be able to make ice, beginning with no ice, when conditions warrant ice growth. For this situation the ice should melt away due to strong entrainment and then the system should remain ice free due to a sustained high value of entrainment. The high entrainment rate should continue deepening even without ice at the surface, although the true deepening rate is probably different than the one represented here with negative ice thickness.

Examining the plot of mixed layer temperature with time reveals that there is more heat storage in the mixed layer beneath freezing conditions (wind speed equals 400 cm/s) at the surface than there is with melting conditions (800-1600 cm/s wind speeds) at the surface. That is, the mixed layer equilibrium temperature is warmer beneath ice growing conditions than it is beneath ice melting conditions. This makes sense when the ice at the surface is thought of as a cap that does not allow the entrained heat to escape out of the system. Since it is not strong enough to melt the ice and cannot escape to the atmosphere, this heat is stored in the mixed layer. Also shown through this sensitivity study is that for a given net heat flux, wind can cause entrainment to be strong enough to melt ice even in freezing atmospheric conditions. Furthermore, strong entrainment can cause and sustain polynya-like conditions.

For the second simulation at h=100 m, the ratio of $\alpha_0 g\Delta T$ to $\beta_0 g\Delta S$ equaled 0.036 for the surface temperature and salinity values. The total heat flux was a constant 0.001 cal/cm^{2}s upward and out of the coupled system. The wind speed was allowed to vary from 400 cm/s to 1600 cm/s in 400 cm/s increments. The results of this wind

sensitivity study show how important the ratio of $\alpha_0 g\Delta T$ to $\beta_0 g\Delta S$ is to entrainment and ice formation or melting.

Like the first simulation, the mixed layer depth increases for all wind speeds due to positive entrainment (Fig.11). The 1600 cm/s wind caused stronger entrainment than the 400 cm/s wind as well. However, for this case the entrainment is never strong enough to melt the ice. Entrainment strength is still dependent on the wind speed, with the higher wind speeds creating greater entrainment. This can be seen in the freezing rate where the lower wind speeds with weaker entrainment have higher freezing rates. In this case the 400 cm/s wind freezes at a rate of approximately 1.1 cm/day (11 cm in ten days) as compared to the 1600 cm/s wind that freezes at a rate of approximately 0.4 cm/day (4 cm in ten days).

Examining the ice thickness time series plot shows that the 1600 cm/s wind slows the freezing rate. Given a few more days with this constant wind speed it is conceivable that the ice formation would halt and that melting might even begin. Salinity predictably increases as freezing occurs at all wind speeds. Here, however, the salinity increases the most for the 1600 cm/s wind as compared to lesser winds. This is in contrast to the result from the first simulation where the greatest freezing rate had the greatest increase in mixed layer salinity. Comparing the 400 cm/s wind to the 1600 cm/s wind and the resulting ice formation of both it is seen that the 400 cm/s wind produces a weaker entrainment, greater ice thickness, and a less saline mixed layer as compared to the 1600 cm/s wind that produces greater entrainment, thinner ice, and a more saline mixed layer.

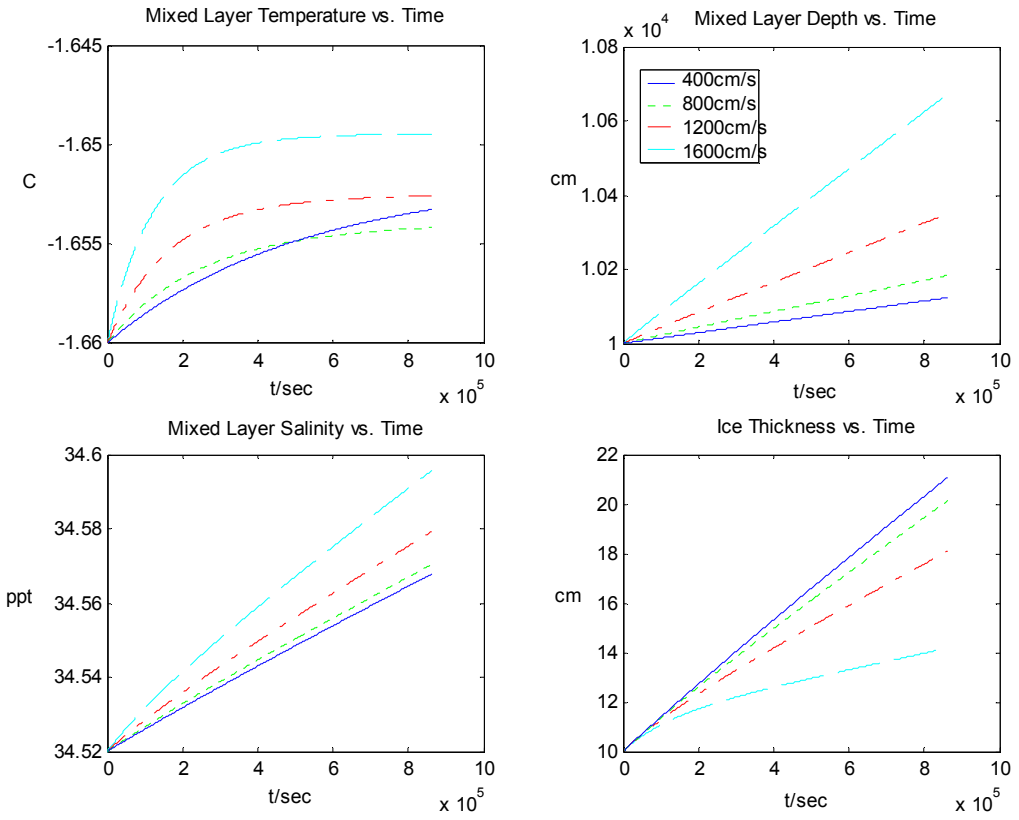

Figure 11. Simulation #2: Sensitivity study for varying winds with h =100 m, Q_0 =0.0010 cal/cm^{2}s, and ratio of $\alpha_0 g\Delta T$ to $\beta_0 g\Delta S$ equal to 0.036. Wind speed changes from 400 cm/s to 1600 cm/s in 400 cm/s intervals.

The 400 cm/s wind is the slowest to bring the system into thermal equilibrium, but appears to achieve a higher equilibrium temperature than some of the greater wind speeds. This can be seen by looking at the mixed layer temperature plot at day ten where the 400 cm/s wind has already surpassed the mixed layer temperature value for the 800 cm/s wind and appears close to exceeding the mixed layer temperature of the 1200 cm/s wind. Like in the first simulation, where ice is present and freezing is occurring, the mixed layer has a higher equilibrium temperature leading to more storage of heat from the effect of ice capping the system. These results indicate that strong entrainment with ice presence will bring the system into thermal equilibrium faster, but that entrainment is not the only factor for establishing what that point of thermal equilibrium will be.

For the third simulation at h=100 m, the ratio of $\alpha_0 g\Delta T$ to $\beta_0 g\Delta S$ again equaled 0.45 for the surface temperature and salinity values. The wind speed was a constant value of 700 cm/s. The heat flux was allowed to vary from 0.0005 cal/cm^{2}s to 0.0025 cal/cm^{2}s in 0.0005 cal/cm^{2}s increments. The results show that for all Q_0 values, sufficient entrainment was produced to deepen the mixed layer (Fig.12). Similar to the second simulation, the stronger the heat flux the greater entrainment it caused and the deeper the mixed layer grew. A low Q_0 value equal to 0.0005 cal/cm^{2}s causes deepening to approximately 103 m, while a Q_0 value equal to 0.0025 cal/cm^{2}s causes deepening to 115 m, for a difference of 12 meters of deepening between the two fluxes.

For all cases of Q_0 the ice actually grows at first but then begins to melt. The time that the transition from freezing to melting occurs differs for each Q_0 value; however, the greater the Q_0 value the longer it takes for this transition to occur. For example, for a heat flux, Q_0 equal to 0.0005 cal/cm^{2}s it takes approximately 1.2 days ($1.0x10^5$ sec) for melting to begin. A heat flux, Q_0, equal to 0.0025 cal/cm^{2}s will take 4.0 days ($3.5x10^5$ sec) for this change from freezing to melting to occur.

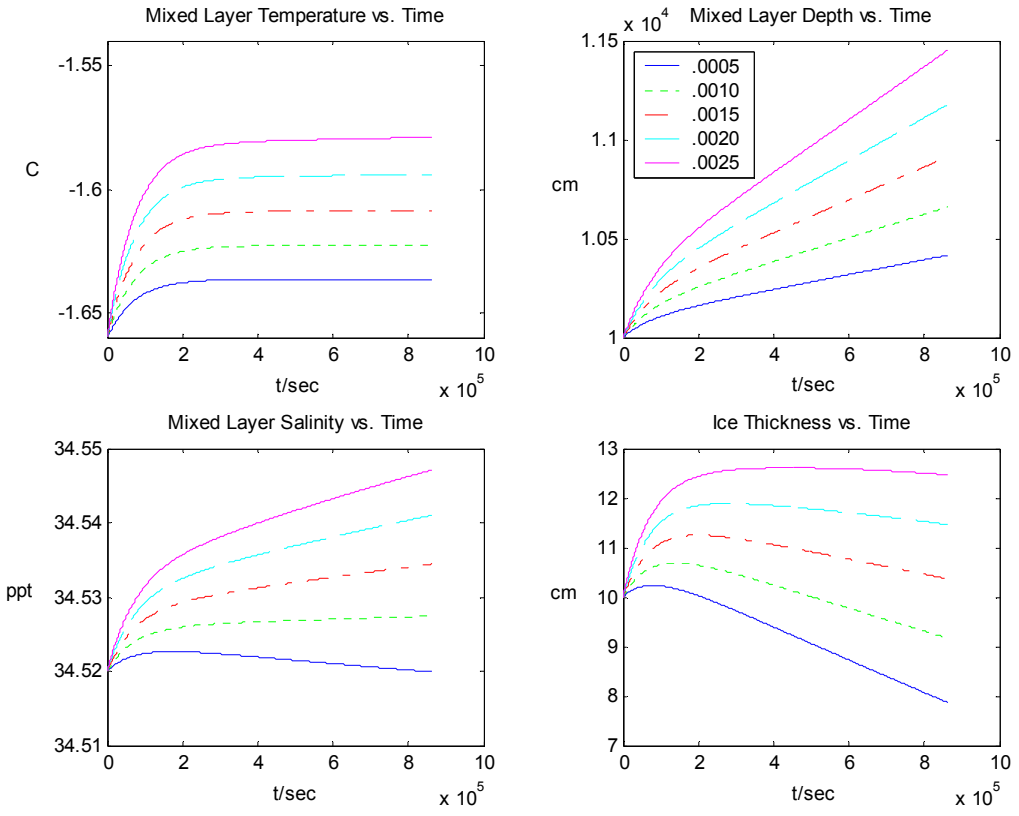

Figure 12. Simulation #3: Sensitivity study for heat fluxes with h =100 m, wind speed =700 cm/s, and ratio of $\alpha_0 g\Delta T$ to $\beta_0 g\Delta S$ equal to 0.45. Heat flux changes from 0.0005 cal/cm^{2}s to 0.0025 cal/cm^{2}s in 0.0005 cal/cm^{2}s intervals.

Mixed layer salinity increases when ice is growing and decreases when ice is melting. This is consistent with the previous two simulations and the physics of salt rejection during ice freezing. When Q_0 equal to 0.0005 cal/cm^{2}s begins melting ice, the salinity predictably starts to decrease, since the melting puts fresh water into the mixed layer. However, at larger values of Q_0 when melting occurs the salinity does not decrease as it does with the Q_0 equal to 0.0005 cal/cm^{2}s; instead, the rate of salinity increase becomes constant. The explanation for this is that entrainment is lifting more salinity into the mixed layer from below than it is taking out of the mixed layer through melting and fresh water addition to the mixed layer.

High heat flux values, like 0.0025 cal/cm^{2}s, that lead to relatively strong freezing had the highest mixed layer equilibrium temperature, and also approached equilibrium faster than lower heat flux values. These results can be observed by comparing Q_0 equal to 0.0005 cal/cm^{2}s with Q_0 equal to 0.0020 cal/cm^{2}s. For 0.0005 cal/cm^{2}s the mixed layer temperature came to equilibrium at approximately -1.64^{o}C after 3.5 days ($3.0x10^5$ sec), while the 0.0020 cal/cm^{2}s heat flux came to equilibrium at approximately -1.597C after 8.7 days ($7.5x10^5$ sec). For these measurements the rate at which the mixed layer temperature comes to equilibrium for the lower heat flux is .0057C/day and the rate at which the mixed layer temperature comes to equilibrium for the higher valued heat flux is .0069C/day. These results suggest that there may be a relationship between ice thickness and heat storage. This relationship would come into practice when strong entrainment does little melting but mixed layer depth continues to increase (deepen). Here, where the ice is not melted and heat cannot escape to the atmosphere, the heat becomes stored in the mixed layer and causes warming of the equilibrium temperature.

Comparing this simulation to the first simulation, where the heat flux was kept constant, produces some interesting results. First, the lowest Q_0 value produces the coolest equilibrium temperature, whereas the lowest wind speed appeared to have the warmest equilibrium temperature. This indicates that more heat can be stored in the mixed layer of the first simulation as compared to the mixed layer of the third simulation for minimum forcing conditions. Second, a 400 cm/s wind with constant Q_0 produced

freezing of ice, but the lowest Q_0 value, 0.0005 cal/cm^{2}s, with constant wind gives melting. Both of these observations can be explained by concluding that the constant values used in simulation are weak enough to allow other factors to influence the entrainment and thus change the characteristics of the coupled system. The usefulness of these constant values for heat flux and wind speed is further substantiated because in simulation 1 where Q_0 is constant and winds are weak, freezing is forecast. Similarly, in simulation 3 where wind speed is constant and Q_0 is weak, melting is forecast.

For the fourth simulation at h=100 m, the ratio of $\alpha_0 g\Delta T$ to $\beta_0 g\Delta S$ equaled 0.036 for the surface temperature and salinity values. The wind speed was a constant value of 700 cm/s. The heat flux was allowed to vary from 0.0005 cal/cm^{2}s to 0.0025 cal/cm^{2}s in 0.0005 cal/cm^{2}s increments. The results demonstrate that positive entrainment causes mixed layer deepening for all heat flux values (Fig.13). The ice thickness growth rate increases as Q_0 increases from 0.0005 cal/cm^{2}s to 0.0025 cal/cm^{2}s with no transition to melting. Salinity predictably increases for all heat flux values, with the strongest rate of salinity increase corresponding to Q_0 equal to 0.0025 cal/cm^{2}s. Like simulation 3, the greatest change in ice thickness is associated with the warmest equilibrium temperature and the largest amount of heat storage within the mixed layer.

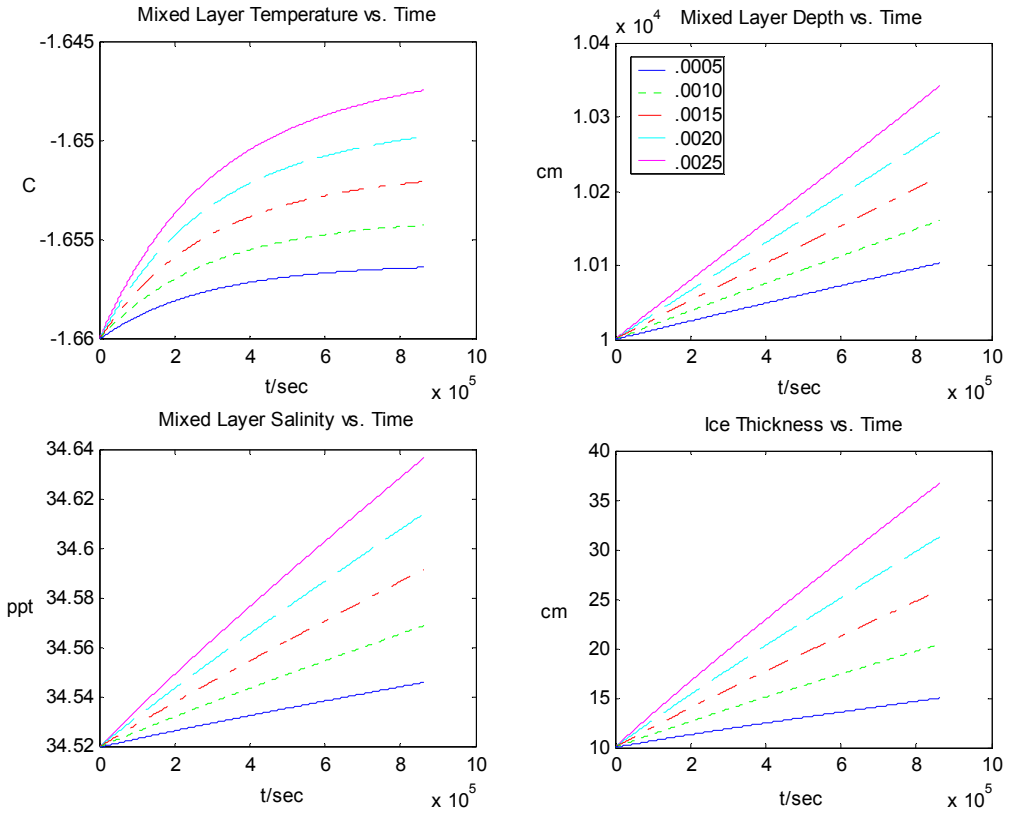

Figure 13. Simulation #4: Sensitivity study for heat fluxes with h =100 m, wind speed =700 cm/s, and ratio of $\alpha_0 g\Delta T$ to $\beta_0 g\Delta S$ equal to 0.036. Heat flux changes from 0.0005 cal/cm^{2}s to 0.0025 cal/cm^{2}s in 0.0005 cal/cm^{2}s intervals.

When comparing this simulation with the previous one the effects of the different ratios of $\alpha_0 g\Delta T$ to $\beta_0 g\Delta S$ can be examined. It appears as though the smaller ratio, 0.036, increases the significance of Q_0 while simultaneously weakening the role of entrainment. A weakening of entrainment would explain why the mixed layer does not deepen as much in simulation 4 as it does in simulation 3. The strongest value for Q_0 in the third simulation deepens the mixed layer to approximately 115 m. The strongest value for Q_0 in the fourth simulation only deepens the mixed layer to 103.5 m. Similarly, the strongest value of Q_0 in the third simulation produces only approximately 11.5 cm of ice, while the strongest value of Q_0 in the fourth simulation produces approximately 37 cm of ice. The fact that the mixed layer temperature remains cooler for each heat flux value in simulation 4 as compared to the same heat flux values in simulation 3 lends credence to the possibility that entrainment has weakened, since less heat is stored in the mixed layer of simulation 4. Further evidence of weakened entrainment is found in the mixed layer salinity versus time plot where for simulation 4 the salinity values for each heat flux value reach higher values than they do in the third simulation. This corresponds to the net effect of increased salt rejection and no addition of fresh water from melting caused by entrained heat.

B. MIXED LAYER DEPTH EQUAL TO 1000 METERS

For the first simulation at h=1000 m, the ratio of $\alpha_0 g\Delta T$ to $\beta_0 g\Delta S$ equaled 0.45 for the surface temperature and salinity values. The total heat flux was a constant 0.001 cal/cm^{2}s up and out of the coupled system. The wind speed was allowed to vary from 400 cm/s to 1600 cm/s in 400 cm/s increments. The results show that positive entrainment deepens the mixed layer for all of the wind speeds (Fig.14). The 400 cm/s wind causes sustained deepening by creating relatively weak entrainment that is not strong enough to melt the ice. The three other larger values for wind cause freezing initially but then shift to melting conditions when entrainment overpowers the net heat flux. This initial freezing period lasts approximately 2.3 days ($2.0x10^5$ sec). After this

period, the mixed layer deepens twice as fast in the 400 cm/s case as it does in the 800 cm/s case.

This rate can be determined by picking values off of the mixed layer depth versus time plot for both the 400 cm/s line and 800 cm/s line corresponding to times of $2.0x10^5$ seconds and $4.0x10^5$ seconds (4.6 days). For the 400 cm/s wind at time equal to $2.0x10^5$ seconds the mixed layer depth equals 1013 m, and at time equal to $4.0x10^5$ seconds the mixed layer depth equals 1021 m. For the 800 cm/s wind at time equal to $2.0x10^5$ seconds the mixed layer depth equals 1010 m, and at time equal to $4.0x10^5$ seconds the mixed layer depth equals 1014 m. Solving for the change in depth per day for each case yields a change of 3.47 m/day for the 400 cm/s wind and a change of 1.74 m/day for the 800 cm/s wind.

The ice thickness versus time plot changes according to the strength of entrainment where greater entrainment causes melting to occur sooner. Predictably, salinity increases with increasing freezing and decreases for strong melting, as is the case with the 1600 cm/s wind. The 400 cm/s wind has the highest equilibrium temperature of the four wind speeds. Conversely, the 1600 cm/s wind has the lowest equilibrium temperature but also achieves thermal equilibrium more quickly than the lesser wind speeds. This result is due to the fact that the high winds produce strong entrainment that is enhanced by thermobaricity to melt the ice without significantly warming the mixed layer. Like thermobaricity, the ratio of mixed layer depth to thermobaric depth likely plays a role in the sustained deepening of the mixed layer for the 400 cm/s wind. The ration of the mixed layer to the thermobaric depth was calculated using depth of the mixed layer, equal to 1000 m, divided by thermobaric depth, which is equal to 93.6 m for all of the simulations.

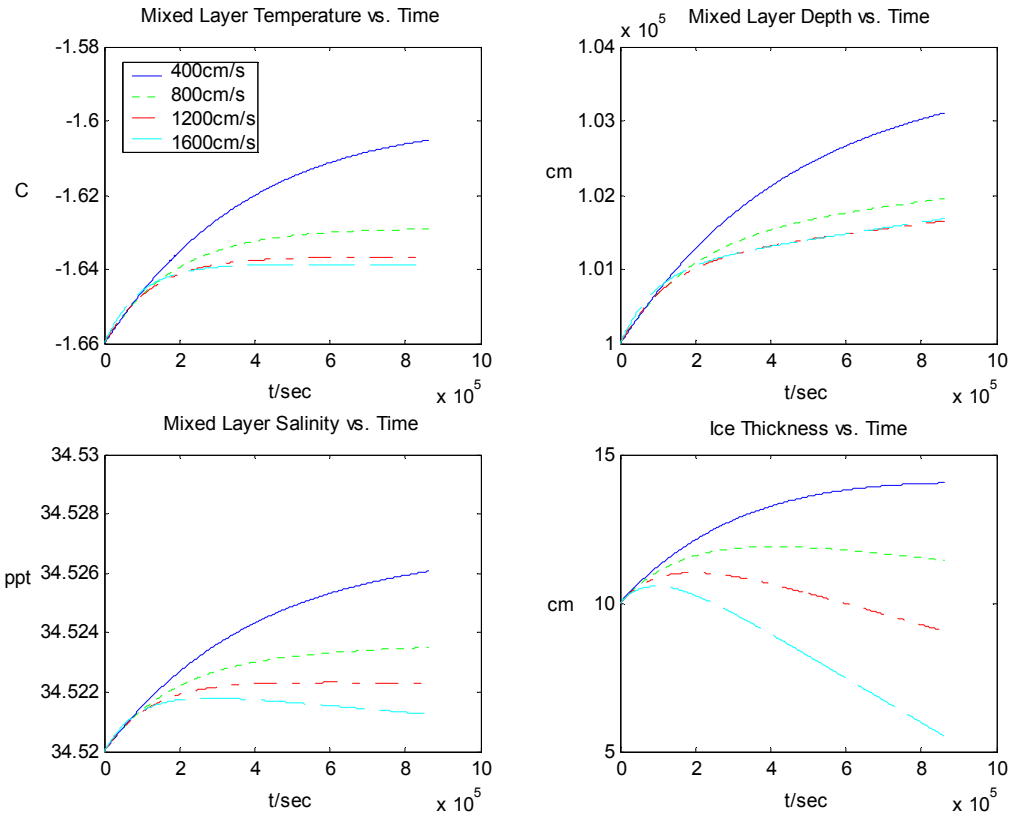

Figure 14. Simulation #5: Sensitivity study for varying winds with h =1000 m, Q_0 =0.0010 cal/cm^{2}s, and ratio of $\alpha_0 g\Delta T$ to $\beta_0 g\Delta S$ equal to 0.45. Wind speed changes from 400 cm/s to 1600 cm/s in 400 cm/s intervals.

For the second simulation at h=1000 m, the ratio of $\alpha_0 g\Delta T$ to $\beta_0 g\Delta S$ equaled 0.036 cal/cm^{2}s for the surface temperature and salinity values. The total heat flux was a constant 0.001 cal/cm^{2}s up and out of the coupled system. The wind speed was allowed to vary from 400 cm/s to 1600 cm/s in 400 cm/s increments. The results show that positive entrainment causes deepening for all cases, where the stronger the wind was the greater the mixed layer deepened (Fig. 15). For this simulation entrainment never became strong enough for melting to occur as evidenced by the constant rates of deepening for all wind speeds. The freezing rate was strongest for the lightest wind but all of the wind speeds had very similar freezing rates. Not surprisingly increase in salinity for all wind speeds was observed.

Looking closely at the temperature scale on the y-axis of the mixed layer temperature versus time plot shows that the mixed layer temperature began near equilibrium and remained relatively constant for this time period. Since there is very little heat storage in the mixed layer with ice present at the surface it seems possible that entrainment is either very weak or has not yet become significant as compared to the net heat flux.

As compared to the previous simulation this simulation's mixed layer does not deepen as much for any of the wind speeds. Similarly, the mixed layer remains cooler and very little heat storage takes place for all the wind speeds in this simulation as compared to the fifth simulation. On average the mixed layer salinity increases more for the sixth simulation than it does for the fifth simulation. However, for the 400 cm/s case the salinity only reaches 34.525 ppt as compared to the slightly more saline value of 34.526 ppt from simulation 5.

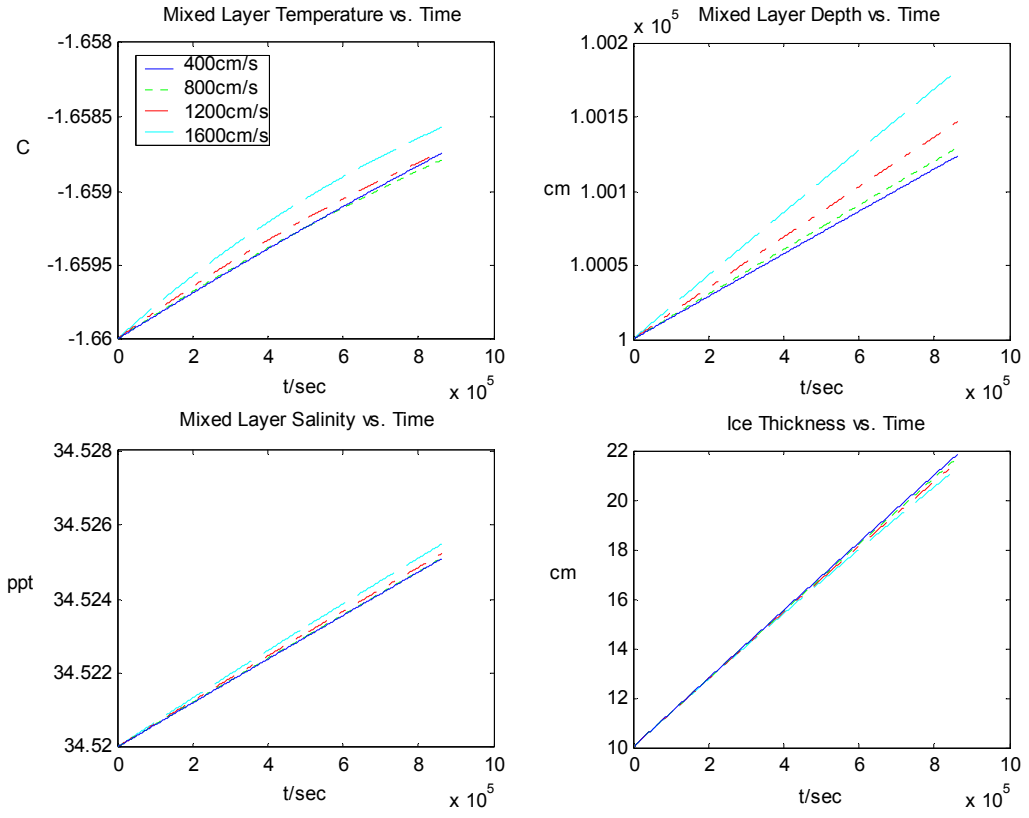

Figure 15. Simulation #6: Sensitivity study for varying winds with h =1000 m, Q_0 =0.0010 cal/cm^{2}s, and ratio of $\alpha_0 g\Delta T$ to $\beta_0 g\Delta S$ equal to 0.036. Wind speed changes from 400 cm/s to 1600 cm/s in 400 cm/s intervals.

For the third simulation at h=1000 m, the ratio of $\alpha_0 g\Delta T$ to $\beta_0 g\Delta S$ equaled 0.45 for the surface temperature and salinity values. The wind speed was a constant value of 700 cm/s. The heat flux was allowed to vary from 0.0005 cal/cm^{2}s to 0.0025 cal/cm^{2}s in 0.0005 cal/cm^{2}s increments. The results show that positive entrainment causes deepening of the mixed layer for all values of Q_0 (Fig.16). There is a greater entrainment for the higher values of heat flux demonstrated by the increased deepening of the mixed layer for the higher values of heat flux. For example, for Q_0 equal to 0.0025 cal/cm^{2}s the mixed layer depth increases to approximately 1055 m, whereas the mixed layer depth for Q_0 equal to 0.0005 cal/cm^{2}s only increases to approximately 1010 m. For all values of Q_0 entrainment causes a shift from freezing to melting conditions. The heat flux equal to 0.0005 cal/cm^{2}s transitions first from freezing to melting at day 4.6 ($4.0x10^5$ sec). Each subsequent heat flux transitions later than its predecessor until Q_0 equal to 0.0025 cal/cm^{2}s transitions at day 5.2 ($4.5x10^5$ sec). This transition occurs more quickly for lower heat flux values because even though the entrainment produced by this low heat flux value is less than the entrainment produced by higher heat flux values, it is more easily overcome by the entrainment.

Salinity follows predictably from the mixed layer depth plot. Again, even though melting occurs the salinity continues to increase due to entrainment of higher salinity water from below. Significant heat storage in the mixed layer can be seen where the mixed layer equilibrium temperature is warmest for the highest Q_0 value. As before, the highest equilibrium temperature appears linked to the highest ice thickness so that entrainment below ice brings heat up into the mixed layer and holds it there while the entrained heat works to melt the ice.

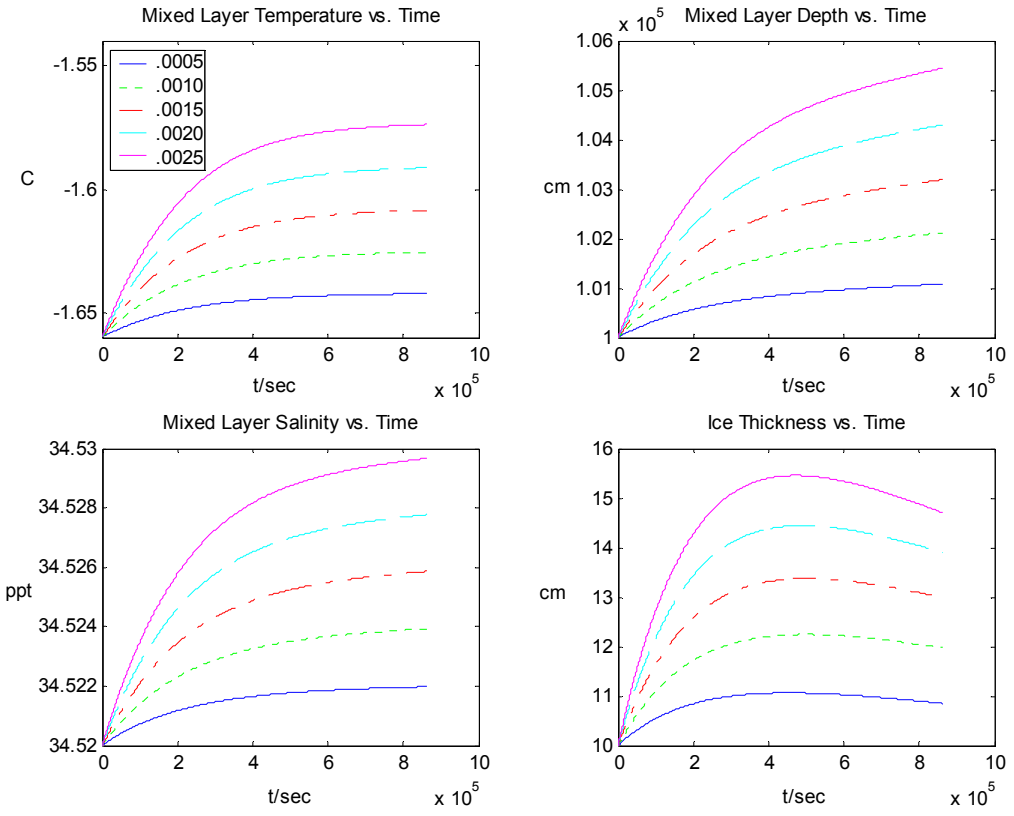

Figure 16. Simulation #7: Sensitivity study for heat fluxes with h =1000 m, wind speed =700 cm/s, and ratio of $\alpha_0 g\Delta T$ to $\beta_0 g\Delta S$ equal to 0.45. Heat flux changes from 0.0005 cal/cm^{2}s to 0.0025 cal/cm^{2}s in 0.0005 cal/cm^{2}s intervals.

Comparing this simulation with simulation 5 so that the effects of keeping Q_0 constant versus keeping wind speed constant produce interesting results. For this simulation the mixed layer depth can increase by as much as 25 m over the maximum mixed layer depth of simulation 5. However, in simulation 5 the maximum depth was produced by the 400 cm/s wind, whereas in this simulation the deepest mixed layer was produced by the 0.0025 cal/cm^{2}s heat flux. This demonstrates that the constant values for Q_0 and wind speed employed are weak enough to allow other factors to influence the entrainment and thus change the characteristics of the coupled system.

Comparing this simulation with the third simulation shows the effects of differing initial mixed layers. The effects include: increased change of mixed layer depth from approximately 15 m for the greatest heat flux in simulation 3, to 55 m for the strongest heat flux in simulation 7; increased maximum salinity value for the greatest heat flux in simulation 3 (34.547 ppt), as compared to the maximum salinity value for the greatest heat flux in simulation 7 (34.530 ppt); and mixed layer equilibrium temperature while relatively constant for all of the heat flux values between the two simulations does increase faster in simulation 3 than in simulation 7, where equilibrium is reached in simulation 3 after approximately 3.5 days ($3.0x10^5$ sec) as compared to 8.7 days ($7.5x10^5$ sec) for simulation 7.

For the fourth simulation at h=1000 m, the ratio of $\alpha_0 g\Delta T$ to $\beta_0 g\Delta S$ equaled 0.036 for the surface temperature and salinity values. The wind speed was a constant value of 700 cm/s. The heat flux was allowed to vary from 0.0005 cal/cm^{2}s to 0.0025 cal/cm^{2}s in 0.0005 cal/cm^{2}s increments. The results show that positive entrainment creates mixed layer deepening for all heat flux values (Fig.17). Entrainment is weak since the mixed layer does not increase much with time (maximum of 3.5 m), freezing occurs for all heat flux cases with the maximum ice thickness equal to 39 cm for Q_0 equal to 0.0025 cal/cm^{2}s, and very little heat can be stored in the mixed layer since the mixed layer temperature varies little even in the most extreme heat flux case (0.003C over 10 days).

Comparing this simulation with simulation 4 (h=100 m) to examine the effects of initial mixed layer depth produces the following: 3.5 meters of depth increase for both simulations where Q_0 equals to 0.0025 cal/cm^{2}s; simulation 8 produces approximately 2 cm more ice for all heat flux cases than simulation 4; the mixed layer temperature warms faster and to larger equilibrium values in simulation 4 than it does in simulation 8; and the mixed layer salinity increases faster and to higher values in simulation 4 than it does in simulation 8. These results can be verified by looking at the slope of the respective lines or by taking sample points off of the lines and comparing the change in a quality over time numerically as done on several occasions above.

Comparing this simulation with simulation 6 to examine the effects of Q_0 versus wind forcing on the deep mixed layer indicates that the effect of strong heat flux values out of the system is more significant to freezing than low wind speeds. This can be quantified by calculating the ice growth from simulation 6 for low wind (400 cm/s) to be equal to 12 cm. Similarly, calculating the ice growth from simulation 8 for high heat flux (0.0025 cal/cm^{2}s) yields 30 cm of ice. From these results it can be concluded that for these values of heat flux and wind speed, large heat flux tends to produce stronger freezing conditions than low wind forcing.

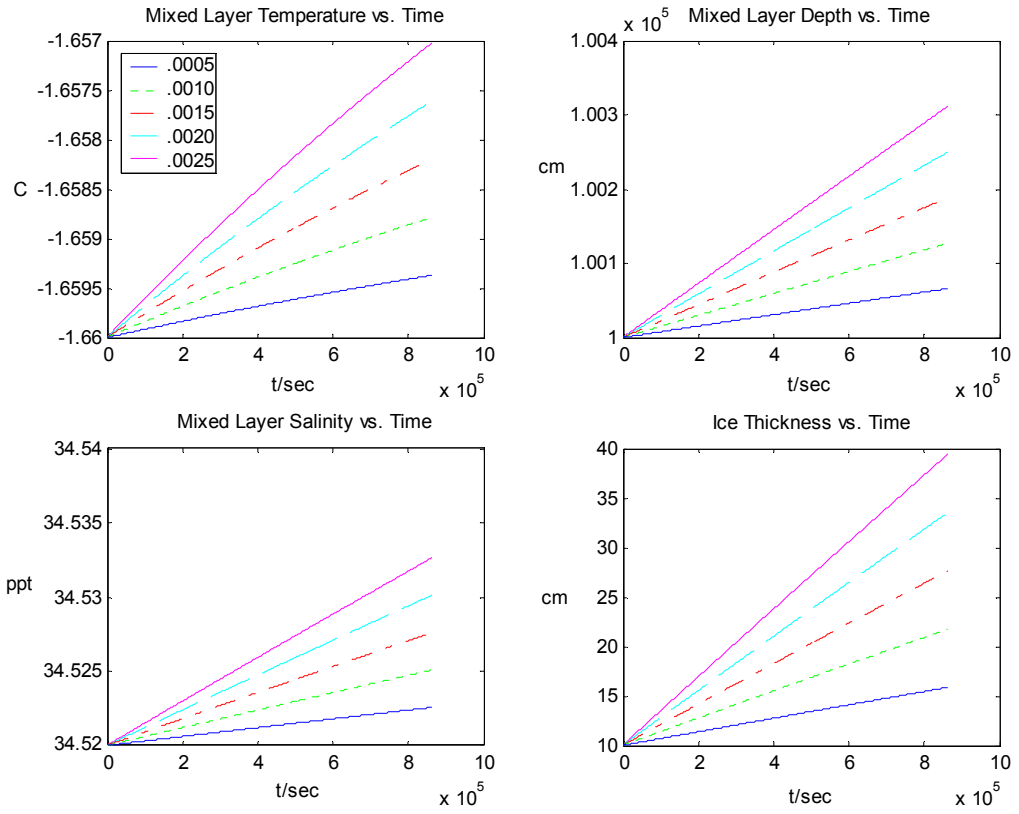

Figure 17. Simulation #8: Sensitivity study for heat fluxes with h =1000 m, wind speed =700 cm/s, and ratio of $\alpha_0 g\Delta T$ to $\beta_0 g\Delta S$ equal to 0.036. Heat flux changes from 0.0005 cal/cm^{2}s to 0.0025 cal/cm^{2}s in 0.0005 cal/cm^{2}s intervals.

Comparing this simulation with simulation 7 to examine the effects of the ratio of $\alpha_0 g\Delta T$ to $\beta_0 g\Delta S$ shows that the higher ratio, like that of simulation 7, produces melting of the ice and greater deepening of the mixed layer (up to 55 m gained as compared to a maximum of 32 m gained in simulation 8). Simulation 7 also can have greater heat storage within the mixed layer as a result of the increased warming of the mixed layer. The mixed layer salinity plots, while reaching similar values for the time length of the simulations, change at different rates. The rate for simulation 8 is nearly linear for all heat flux values and is equal to .0013ppt/day for Q_0 equal to 0.0025 cal/cm^{2}s. The rate for simulation 7 is not linear since the entrainment for this simulation is strong enough to cause a transition between freezing and melting conditions. This rate is equal to 0.001ppt/day for Q_0 equal to 0.0025 cal/cm^{2}s. While this difference in rates appears small, examination of the plots shows that for simulation 7 the rate appears to tend toward equilibrium and may, after a long enough period, become negative or decrease the salinity of the mixed layer. Meanwhile, the rates for the various heat fluxes in simulation 8 constantly increase the salinity of the mixed layer. Ultimately, comparing the results of simulation 8 with simulation 7 suggest that the low ratio of $\alpha_0 g\Delta T$ to $\beta_0 g\Delta S$ from simulation 8 cannot support as strong an entrainment rate as the higher ratio of $\alpha_0 g\Delta T$ to $\beta_0 g\Delta S$ from simulation 7.

V. CONCLUSIONS

A. SUMMARY

The coupled ice-mixed layer system is a delicate balance of physical processes that are dependent on both initial conditions and forcing conditions. Changes in the heat and or buoyancy fluxes, wind speed, initial ice thickness, and initial mixed layer depth can all initiate feedback processes that can lead to either ice growth or melting. This balance of physical processes is so tenuous that a moderate change in any quantity or combination of quantities rarely produces an intuitive result. Based on this balance it is easy to understand why different basins in the Arctic at constant latitude can have different amounts of ice thickness at the surface. Similarly, polynya formation and maintenance is better understood in light of these intricate relationships. Ultimately, ice formation or melting cannot be forecast from surface forcing conditions alone, as has been attempted in the past. Thorough knowledge of the site-specific temperature and salinity profiles and fluxes are necessary in conjunction with the surface forcing conditions to predict entrainment and ice thickness.

Thermobaricity is a real and significant factor for quantifying the strength of entrainment and the turbulent kinetic energy of the coupled system. In comparing simulations between different initial mixed layer depths the thermobaricity seems particularly important or sensitive to wind forcing as compared with changing heat fluxes. In other words, the greatest changes in mixed layer depths were found for the varying wind cases with an initial mixed layer depth of 1000 m. For these cases the change in mixed layer depth could be as large as 60 m. The comparable case for initial mixed layer depth of 100 m could only achieve a maximum of 15 m. (To see these maximum possible depths compare Figures 12 and 16.) This scenario is especially important for sustaining polynya events and indicates that perhaps surface wind forcing does more to maintain polynya conditions than net surface heat flux. Furthermore, this mechanism for rapid and strong deepening of the mixed layer is important because it likely helps explain deep-water regeneration on a global scale.

Another significant result of the simulations was an observed relation between greater ice thickness and higher heat storage in the mixed layer. In particular as described above every simulation shows that for the greatest freezing rate it takes the mixed layer temperature longer to come into equilibrium and thus stores and holds on to more heat as it comes into equilibrium. Simulation 2 and simulation 6 (in Figures 11 and 15, respectively) appear to be exceptions to the rule, however. For their given conditions it appears that the simulation did not run long enough to allow the mixed layer temperature to come into equilibrium. This can be seen where the plots are still rising up and starting to bend toward equilibrium. This result is significant because it indicates that thick ice at the surface acts as a cap on the coupled system. This cap does not stop entrainment from melting the ice at the surface; instead, melting begins before the system comes to thermal equilibrium indicating that when there is ice at the surface the entrained heat works to melt the ice before it works to warm the mixed layer.

Perhaps the most significant result of the simulations was to verify the complexity of the interactions that occur in the coupled system and which are represented in the equations developed in the theory section. For example, as predicted by the equations, no one factor was determined to be the most important to quantify for determining entrainment strength. Instead, because of the feedbacks inherent in the system, a condition that led to strong entrainment in one case may not lead to strong entrainment in another case, depending on the other initial and forcing conditions. Because of these feedbacks, it is critical that modeling of coupled ice-mixed layer system include the realistic thermodynamics described above. Similarly, this work has demonstrated that the PIPS model would become significantly more useful for ice prediction if the necessary physics were included.

B. RECOMMENDATIONS FOR FURTHER STUDY

There are many possible topics of further study for high latitude mixed layer dynamics and thermodynamics. Preconditioning for polynyas by advective processes at depth like warm subsurface eddies, as mentioned by both Hakkinen (1987) and Lemke *et al.,* (1990), should be explored as a possible mechanism to aid entrainment in polynya

initiation and maintenance. From an atmospheric perspective, further research of the effects of precipitation in ice-free and ice-covered regions is important for greater resolution of heat flux data and the total energy balance. Net surface heat flux into the system needs to be thoroughly explored just as net heat flux out of the coupled system was examined in this work. Similar sensitivity studies of net heat flux both into and out of the coupled system need to be conducted for an initial ice thickness value equal to zero. For this study it is critical that the model be able to transition freely and correctly between the ice-free system and the ice-covered system.

THIS PAGE INTENTIONALLY LEFT BLANK

LIST OF REFERENCES

Aagaard, K. and E.C. Carmack. The arctic ocean and climate: a perspective, in *The Role ofthe Polar Oceans in Shaping the Global Environmen*t, O. Johannessen, R. Muench and J.Overland, Eds., Geophysical Monograph 85, pp.5-20, 1994.

Akitomo, K. Open-ocean deep convection due to thermobaricity, 2, numerical experiments. *J.Geophys. Res.*, 104, 5235-5249.

Barry, R.G., M.C. Serreze, J.A. Maslanik, and R.H. Preller. The arctic sea ice-climate system: observations and modeling. *Review of Geophysics*, 31, 397-422, 1993.

Coachman, L.K. and K. Aagaard, Physical Oceanography of Arctic and Subarctic Seas, Chapter 1, in Marine Geology and Oceanography of the Arctic Seas, Y. Herman, ed., 1-72, Springer-Verlag, N.Y., 1974.

Garwood, R.W., Jr. An oceanic mixed layer model capable of simulating cyclic states. *J. Phys. Oceanogr*., 7, 455-471, 1977.

Garwood, R.W., Jr. Enhancements to deep turbulent entrainment. In *Deep Convection and Deep Water Formation in the Ocea*n, Ed. by P. C. Chu and J. C. Gascard, Elsevier, 189-205, 1991.

Garwood, R.W., Jr. Critical mixed layer depth for maintaining convective polynyas. International Polynya Symposium, Quebec City, September, 2001.

Garwood, R.W., Jr. Thermodynamics Critical to Arctic Mixed Layer Systems, Small-Scale Sea Ice Ocean Modeling (SIOM) Workshop, Fairbanks, August, 2002.

Garwood, R.W., Jr. And S. Isakari. Entropy Conserving deep convection in the Weddell Sea. *Proceedings Fourth International Conf. Southern Hemisphere Meteorol. and Oceanog*r., Hobart, 29 March - 2 April, 503-504, 1993.

Garwood, R.W., Jr., S.M. Isakari, and P.C. Gallacher. Thermobaric convection, in *The Role of the Polar Oceans in Shaping the Global Environmen*t, O. Johannessen, R. Muench and J. Overland, Eds., Geophysical Monograph 85, pp.199-209, 1994.

Gill, A.E., and J.S. Turner. A comparison of seasonal thermocline models with observations. *Deep-Sea Res.,* 23, 391-401, 1976.

Hakkinen, S. A coupled dynamic-thermodynamic model of an ice-ocean system in the marginal ice zone. *J. Geophys. Res*., 92, 9469-9478, 1987.

Hibler, W.D.. A dynamic thermodynamic sea ice model. *J. Phys. Oceanogr*., 9, 817-846, 1979.

Jiang, L. and R.W. Garwood, Jr. A numerical study of three-dimensional dense bottom plumes on a southern ocean continental slope. *J. Geophys. Re*s., 100, 18471-18488, 1995.

Jiang, L. and R.W. Garwood, Jr. Three-dimensional simulations of overflows on continental slopes. *J. Phys. Oceanog*r., 26, 1214-1233, 1996.

Jiang, L. and R.W. Garwood, Jr. Effects of topographic steering and ambient stratification on overflows on continental slopes: A model study. *J. Geophys. Re*s., 103, 5459-5476, 1998.

Kraus, E.B. And J.S. Turner. A dynamic thermodynamic sea ice model. *Tellu*s, 19, 98-105, 1967.

Large, W.G., J.C. McWilliams and S.C. Doney. Oceanic vertical mixing: A review and a model with a nonlocal boundary layer parameterization. *Rev Geophys*., 32, 363-403, 1994.

Lemke, P., W.B. Owens and W.D. Hibler, III. A coupled sea ice-mixed layer -pycnocline model for the Weddell Sea. *J. Geophys. Res*., 95, 9513-9525, 1990. .

Martinson, D.G., P.D. Killworth, and A.L. Gordon. A convective model for the Weddell Polynya. *J. Phys. Oceanogr*., 11, 466-488, 1981.

MathWorks, Inc. Natick, MA, 2002.

McDougall, T.J., The relative roles of diapycnal and isopycnal mixing on subsurface water mass conversion. *J. Phys. Oceanogr.,* 14, 1577-1589, 1984.

Mellor, G.L. and S. Hakkinen. A review of coupled ice-ocean models, in *The Role of the Polar Oceans in Shaping the Global Environmen*t, O. Johannessen, R. Muench and J. Overland, Eds., Geophysical Monograph 85, pp.21-31, 1994.

Mellor, G L. And T. Yamada, Development of a turbulence closure model for geophysical fluid problems. *Rev. Geophy*s, 20, 8510875, 1982.

Okada, I. and T. Yamanouchi. Seasonal change of the atmospheric heat budget over the southern ocean from ECMWF and ERBE data in 1988, in *Proceedings of the NIPR Symposium on Polar Meteorology and Glaciology,* 9, 146-159, 1995.

Preller, R.H., P.G. Posey, W. Maslowski, D. Stark and T.T.C. Pham. Navy sea ice prediction systems. *Oceanograph*y, Vol. 15, 44-56, 2002.

Rudels, B., E.P. Jones, L.G. Anderson, and G. Kattner. On the intermediate depth waters of the arctic ocean, in *The Role of the Polar Oceans in Shaping the Global Environmen*t,

O. Johannessen, R. Muench and J. Overland, Eds., Geophysical Monograph 85, pp.33-46, 1994.

Shampine, L.F. Numerical Solution of Ordinary Differential Equations. Chapman & Hall, 1994.

Smith, S.D., R.D. Muench, and C.H. Pease. Polynyas and leads: An overview of physical processes and environment. *J. Geophys. Res*., 95, 9461-9479, 1990.

Vihma, T. Subgrid parameterization of surface heat and momentum fluxes over polar oceans. *J. Geophys. Res.,* 100, 22625-22646, 1995.

Walsh, J.E. and C.M. Johnson. An analysis of Arctic Sea Ice Fluctuations, 1953-77. *J. Phys. Oceanogr.,*9, 580-591, 1979.

Wu, X., I. Simmonds, and W.F. Budd. Southern hemisphere climate system recovery from 'instantaneous' sea-ice removal. *Q.J.R. Meteorological Society,* 122, Second Proof, 1996.

THIS PAGE INTENTIONALLY LEFT BLANK

INITIAL DISTRIBUTION LIST

1. Defense Technical Information Center
   Ft. Belvoir, Virginia

2. Dudley Knox Library
   Naval Postgraduate School
   Monterey, California

3. Dr. Dennis M. Conlon, Program Manager
   High Latitude Dynamics Program, Code 322HL
   Office of Naval Research
   Arlington, Virginia

4. Prof. R.W. Garwood
   Naval Postgraduate School
   Monterey, California

5. Prof. Peter Guest
   Naval Postgraduate School
   Monterey, California

6. Prof. Arlene Guest
   Naval Postgraduate School
   Monterey, California

7. Prof. Tim Stanton
   Naval Postgraduate School
   Monterey, California

8. ENS Mathias Roth
   Naval Postgraduate School
   Monterey, California